TRANSITION PATH THEORY FOR LANGEVIN DYNAMICS ON MANIFOLDS: OPTIMAL CONTROL AND DATA-DRIVEN SOLVER*

YUAN GAO†, TIEJUN LI‡, XIAOGUANG LI§, AND JIAN-GUO LIU¶

Abstract. We present a data-driven point of view for rare events, which represent conformational transitions in biochemical reactions modeled by overdamped Langevin dynamics on manifolds in high dimensions. We first reinterpret the transition state theory and the transition path theory from the optimal control viewpoint. Given a point cloud probing the manifold, we construct a discrete Markov chain with a Q-matrix computed from an approximated Voronoi tesselation via the point cloud. We use this Q-matrix to compute a discrete committor function whose level set automatically orders the point cloud. Then based on the committor function, an optimally controlled random walk on point clouds is constructed and utilized to efficiently sample transition paths, which become an almost sure event in $O(1)$ time instead of a rare event in the original reaction dynamics. To compute the mean transition path efficiently, a local averaging algorithm based on the optimally controlled random walk is developed, which adapts the finite temperature string method to the controlled Monte Carlo samples. Numerical examples on sphere/torus including a conformational transition for the alanine dipeptide in vacuum are conducted to illustrate the data-driven solver for the transition path theory on point clouds. The mean transition path obtained via the controlled Monte Carlo simulations highly coincides with the computed dominant transition path in the transition path theory.

Key words. reaction rates, most probable path, committor function, controlled Markov process, realize rare events almost surely, nonlinear dimension reduction

MSC codes. 60J22, 65C05, 60H30, 93E20

DOI. 10.1137/21M1437883

1. Introduction. Complex molecular dynamics in chemical/biochemical reactions usually have cascades of time scales. For instance, the molecular vibrations occur in a femtosecond time scale, while the conformational transitions occur in a microsecond time scale. Assume the states $\{\mathbf{x}(t)\}$ of the original molecular dynamics are in a high dimensional space $\mathbb{R}^p$, and suppose the most important slow dynamics such as conformational transitions can be described by a reduced overdamped Langevin dynamics in terms of reaction coordinates $\mathbf{y}$ on an intrinsic low-dimensional manifold $\mathcal{N} \subset \mathbb{R}^\ell$, where $\ell \ll p$ [CL06]. Then the slow dynamics on $\mathcal{N}$ is guided by a reduced free energy $U_{\mathcal{N}}(\mathbf{y})$, $\mathbf{y} \in \mathcal{N}$, whose local minima indicate several metastable states (say a, b) of the dynamics. Those conformational transitions from one metastable state a

---

†Department of Mathematics, Purdue University, West Lafayette, IN 47906 USA (gao662@purdue.edu).

‡LMAM and School of Mathematical Sciences, Peking University, Beijing 100871, China (tieli@pku.edu.cn).

§MOE-LCSM, School of Mathematics and Statistics, Hunan Normal University, Changsha 410081, China (lixiaoguang@hunnu.edu.cn).

¶Department of Mathematics and Department of Physics, Duke University, Durham, NC 27708 USA (jliu@math.duke.edu).

to another metastable state b are rare (but significant) events compared with typical relaxation dynamics in each energy basin. Thus efficient simulation and computation of transition rates or reaction pathways for the conformational transitions are challenging and important problems, which has been one of the core subjects in applied mathematics in recent years; see the recent review in [EVE10].

To make the discussion precise, we denote the overdamped Langevin dynamics of $\mathbf{y}_t$ by

$$(1.1) \qquad d\mathbf{y}_t = -\nabla_{\mathcal{N}} U_{\mathcal{N}}(\mathbf{y}_t)\, dt + \sqrt{2\varepsilon} \sum_{i=1}^{d} \tau_i^{\mathcal{N}}(\mathbf{y}_t) \otimes \tau_i^{\mathcal{N}}(\mathbf{y}_t) \circ dB_t,$$

where $\varepsilon > 0$ corresponds to the thermal energy in physics, the symbol $\circ$ means the Stratonovich integration, B_t is ℓ-dimensional Brownian motion, d is the intrinsic dimension of the manifold $\mathcal{N}$, and $\{\tau_i^{\mathcal{N}}; 1 \le i \le d\}$ are orthonormal bases of tangent plane $T_{\mathbf{y}_t}\mathcal{N}$. Here $\nabla_{\mathcal{N}} := \sum_{i=1}^{d} \tau_i^{\mathcal{N}} \nabla_{\tau_i^{\mathcal{N}}} = \sum_{i=1}^{d} \tau_i^{\mathcal{N}} \otimes \tau_i^{\mathcal{N}} \nabla$ is the surface gradient and $\nabla_{\tau_i^{\mathcal{N}}} = \tau_i^{\mathcal{N}} \cdot \nabla$ is the tangential derivative in the direction of $\tau_i^{\mathcal{N}}$. Given the manifold $\mathcal{N}$ and potential $U_{\mathcal{N}}(\mathbf{y})$, when ε is small, the study of rare events by direct simulation of (1.1) is not feasible. This motivates the need for theoretical developments. In the limit $\varepsilon \to 0$, the optimal transition path problem can be well described through the large deviation theory [FW12]. This was formulated as the minimum action method (MAM) [ERVE04] and was extended to the manifold case in [LLZ16]. In the gradient case, the optimal transition path by MAM is actually the minimal energy path (MEP) connecting two metastable states, which was realized by the string method [ERVE02]; see also recently developed computational methods for the zero noise transition paths [VEH08, HVE08, GVE17, GVE19]. The string method was further extended to the finite ε case, i.e., the finite temperature string method for gradient systems [ERVE05]. In the general finite noise case, the transition path theory (TPT) was first proposed by E and Vanden-Eijnden in [EVE06] to obtain the transition paths and transition rates, etc., by the committor function q (see (3.3)). A mathematically rigorous interpretation of TPT was given in [LN15] (see precise statement in [LN15, Theorem 1.7]). The generalization of TPT to Markov jump process was given in [MSVE09].

We are concerned with the rare event study from a data-driven point of view in this paper. In many cases, the manifold $\mathcal{N}$ is not explicitly known, and we assume only the point clouds $\{\mathbf{x}_i\}_{i=1:n}$ are available from some physical dynamics on an unknown d dimensional closed smooth Riemannian submanifold $\mathcal{M} \subset \mathbb{R}^p$. We assume there are well-distributed data points probing the manifold, so one can learn the reaction coordinates $\mathbf{y} = \Phi(\mathbf{x}) : \mathcal{M} \hookrightarrow \mathbb{R}^{\ell}$ by using $\{\mathbf{x}_i\}_{i=1:n}$ in $\mathbb{R}^p$. Thus $\mathcal{N} = \Phi(\mathcal{M})$ is a d dimensional closed smooth submanifold of $\mathbb{R}^{\ell}$ and one can represent the high dimensional data $\{\mathbf{x}_i\} \subset \mathcal{M} \subset \mathbb{R}^p$ as $\{\mathbf{y}_i\} = \{\Phi(\mathbf{x}_i)\} \subset \mathcal{N} \subset \mathbb{R}^{\ell}$ in the low dimensional space. In general, this dimension reduction step is very challenging. Besides the standard diffusion map nonlinear dimension reduction [CL06], some reinforced learning methods based on built-in domain knowledge have recently been developed; cf. [ZWE18]. As for a real example, we simulate a simple, manageable alanine dipeptide with 22 atoms to collect a full atomic molecular dynamics result for $\mathbf{x} \in \mathbb{R}^{66}$. Its lower energy states are mainly described by two backbone dihedral angles $\phi \in [-\pi, \pi)$ and $\psi \in [-\pi, \pi)$, so the reaction coordinate $\mathbf{y}$ is chosen to be in a torus $\mathcal{N} \subset \mathbb{R}^3$; see Figure 6 and Example 3 below. With the learned reaction coordinate $\mathbf{y}$, the main goal is to effectively simulate the conformational transitions on $\mathcal{N}$.

Our main contribution is twofold: (i) We give the *stochastic optimal control reinterpretations of the committor function* in TPT; (ii) adapting an idea similar to the

finite temperature string method, we *propose a data-driven solver for finding a mean transition path on manifold, which is constructed using the level-set defined by the committor function and taking advantage of an optimally controlled Monte Carlo simulation.* Details are presented below.

Interpretation from optimal control viewpoint. The study of rare events from the optimal control viewpoint was pioneered in [HS12, HBS$^+$13] and further investigated in [HSZ16, HRSZ17]. Our goal in the first part is to rigorously reformulate the effective conditioned process—constructed from committor function q by [LN15]—as a stochastic optimally controlled process, in which the optimal feedback controls the original Markov process from one stable absorbing set A to another absorbing set B of the energy landscape $U_{\mathcal{N}}$ with minimum cost. Compared with the infinite optimal terminal time $T = +\infty$, the corresponding stochastic optimal control problem at a fixed noise level $\varepsilon > 0$ is indeed easier in the sense that the stopping time (the stochastic terminal time) is almost surely finite $\tau < +\infty$. Thus the stochastic optimal control reinterpretation enables feasible computation of transition paths for practical scientific problems. Precisely, for the system described by a Markov process $\mathbf{y}_t$ on manifold $\mathcal{N}$, e.g., (1.1), it will induce a measure on the path space $C([0, +\infty); \mathcal{N})$, which can be regarded as a prior measure P. Then we need to construct a controlled Markov process $\tilde{\mathbf{y}}_t$ (see (3.20)), which induces a new measure $\tilde{P}$ on the path space. The additional control drives the trajectory $\tilde{\mathbf{y}}_t$ from A to B almost surely, while the transitions for the original process are rare events. From the stochastic optimal control viewpoint, we need to find a control function $\mathbf{v}(\tilde{\mathbf{y}}_t)$ to realize the optimal change of measure from P to $\tilde{P}$ such that the running cost (kinetic energy) and terminal cost (boundary cost hitting the absorbing set) are minimized. In Theorem 3.3 in section 3.2, we will first prove a regularized stochastic optimal control problem with a terminal cost N on stable basin $\bar{A}$ which prevents $\tilde{\mathbf{y}}_t$ from hitting on A before B. Then the regularized forward committor function q_{N} gives an optimal control $\mathbf{v}_{\text{N}}^* = 2\varepsilon\nabla \ln q_{\text{N}}$ that realizes the optimal change of measure on path space and thus realizes the transitions from A to B almost surely. The monotone dependence on the cut-off N for q_N and the associated value function and the effective equilibrium are also proved. Thus we justify that the committor function, as the limit of the regularized q_{N}, provides the optimal control and the effective equilibrium which drive $\tilde{\mathbf{y}}_t$ from A to B almost surely. These results also provide the basis for computing the transition path through the Monte Carlo simulations for the controlled random walk, constructed from the effective equilibrium $\pi^e = \pi q^2$, and the local average mean path algorithm in the second part.

Data-driven solver for mean transition path on manifolds. Our goal in this part is to take the advantage of the optimal control reinterpretation above in its discrete analogies to design a data-driven solver, which efficiently finds a mean transition path on a manifold suggested by point clouds. Given the point clouds $\{\mathbf{y}_i\}_{i=1:n}$, we construct a discrete Markov chain on $\{\mathbf{y}_i\} \subset \mathcal{N}$ based on an approximated Voronoi tesselation for $\mathcal{N}$, which incorporates both the equilibrium and manifold information. The assigned transition probability between the nearest neighbor points (adjacent points identified by Voronoi tesselation) enables us to efficiently compute the discrete committor function $\{q_i\}_{i=1:n}$ and related quantities. In section 4.2, based on the constructed discrete Markov chain, we derive an optimally controlled Markov process on point clouds with the associated controlled generator Q^q. More importantly, the corresponding effective equilibrium under control is simply given by $\pi^e \propto q^2\pi$, which preserves the detailed balance property. First, this enables an efficient controlled Monte Carlo simulations for the new almost sure event in $O(1)$ time instead of the

rare event in the original process. Moreover, adapting the idea from the finite temperature string method [ERVE05, RVEME05], we use a Picard iteration to find the mean transition path based on the controlled Monte Carlo samplers. The numerical construction of the optimally controlled random walk is given in section 4.2, while the TPT analysis and the local average mean path algorithms based on the controlled process sampling are given in section 5. We apply this methodology to simulate the rare transitions on sphere/torus with Mueller potential and the transition between different isomers of an alanine dipeptide with MD simulation data. The developed mean transition path algorithm based on the controlled process performs very well for both synthetic and real-world examples, which highly coincide with the computed dominant transition path in TPT.

The rest of this paper is organized as follows. In sections 2 and 3, we will make the connections between the optimal control theory and the transition state theory and the transition path theory, respectively. In section 4, we present the constructions of the discrete original/controlled Markov process on point clouds. In section 5, we present the detailed algorithms for finding mean transition paths, while in section 6 numerical examples are conducted to show the validity of the proposed algorithms.

2. Preliminaries: Energy landscape and terminologies for stochastic optimal control. In this section, we will first consider the typical energy landscape $U_\mathcal{N}$ which indicates two metastable states and guides the Langevin dynamics on $\mathcal{N}$ (see section 2.1). Then in section 2.2, we briefly review the basic concepts for a stochastic optimal control problem in the infinite time horizon.

2.1. Energy landscape in the transition state theory. A chemical reaction from reactants $a \in \mathcal{N}$ through a transition state $c \in \mathcal{N}$ to products $b \in \mathcal{N}$ can be described by the reaction coordinate $\mathbf{y}$ and a path on the reaction coordinate $\mathbf{y}(t) \in \mathcal{N}$ with a pseudo-time $t \in [0, T]$ and $\mathbf{y}(0) = a$, $\mathbf{y}(T) = b$. This chemical reaction can be characterized by an underlying potential $U_\mathcal{N}(\mathbf{y})$ in terms of the reaction coordinate $\mathbf{y} \in \mathcal{N}$, which is assumed to be smooth enough and has a few deep wells separated by high barriers. Assume a and b are two local minima (attractors) with the basins of attractors A, $B \subset \mathcal{N}, A \cap B = \emptyset$ and $\max(U_\mathcal{N}(a), U_\mathcal{N}(b)) < \min U(\partial A \cup \partial B)$. The associated minimal energy barrier such that $\mathbf{y}(0) = a$, $\mathbf{y}(T) = b$ is given by $\min_{\mathbf{y}(\cdot)} (\max_{t \in [0,T]} U_\mathcal{N}(\mathbf{y}(t)))$. Then pick a path $\mathbf{y}^*(\cdot) \in \mathrm{argmin}_{\mathbf{y}(\cdot)}(\max_{t \in [0,T]} U_\mathcal{N}(\mathbf{y}(t)))$, and define

$$(2.1) \qquad c = \mathrm{argmax}_{\mathbf{y}^*(t), t \in [0,T]} U_\mathcal{N}(\mathbf{y}^*(t)).$$

This state c achieves the minimal energy barrier, and we assume this type of c, called the transition state, is unique. Moreover, assume $U_\mathcal{N}$ is a Morse function and the Morse index at saddle point (transition state c) is 1, i.e., there is only one negative eigenvalue for the Hessian matrix of $U_\mathcal{N}$ in the neighborhood of c. The energy barrier to achieve the chemical reaction from a to b is $U_\mathcal{N}(c) - U_\mathcal{N}(a)$. With this assumption, the minimal energy path can be uniquely found from the following least action problem [FW12]:

$$(2.2) \qquad S(A, B) = \inf_{T>0} \ \inf_{\mathbf{y} \in C[0,T]; \mathbf{y}(0)=a, \mathbf{y}(T)=b} \int_0^T \frac{1}{2} |\dot{\mathbf{y}} + \nabla U_\mathcal{N}(\mathbf{y})|^2 \, \mathrm{d}t.$$

For notational simplicity, from now on we use U as shorthand notation for $U_\mathcal{N}$, ∇ as shorthand notation for $\nabla_\mathcal{N}$, and $\nabla\cdot$ as shorthand notation for the surface divergence defined as $\nabla_\mathcal{N} \cdot \xi = \sum_{i=1}^d \tau_i^\mathcal{N} \cdot \nabla_{\tau_i^\mathcal{N}} \xi$. In the case that U is a double-well potential

with a, b being two local minima, the minimal energy path (MEP) is given by the combination of the solutions $\mathbf{y}(t), t \geq 0$, to [FW12]

$$(2.3) \quad \begin{aligned} \dot{\mathbf{y}} &= \nabla U(\mathbf{y}), \quad \mathbf{y}(-\infty) = a, \mathbf{y}(+\infty) = c, \\ \dot{\mathbf{y}} &= -\nabla U(\mathbf{y}), \quad \mathbf{y}(-\infty) = c, \mathbf{y}(+\infty) = b. \end{aligned}$$

The MEP is formulated as an exit time problem computed by finding out a quasi-potential from a Hamilton–Jacobi equation [FW12]. We refer the reader to [ERVE02, ERVE04, VEH08, HVE08, GVE17, GVE19] for various computational methods for the MEP and the deterministic optimal control interpretations of the zero-noise limit path.

At the finite noise level, one can directly use committor function q defined in (3.3) instead of the quasi-potential, and solving the committor function is a linear problem. In the next section, we reinterpret the transition path theory from the stochastic optimal control viewpoint and then use the optimal control to efficiently compute the transition path at a finite noise level. Before that, we first introduce general terminology of stochastic optimal control.

2.2. General stochastic optimal control problems with terminal cost. In general, one can consider a stochastic optimal control problem with some running cost function $L(\mathbf{y}_t, \mathbf{v}_t)$ and terminal cost function $g(T, \mathbf{y}_T)$, where we have used the convention $\mathbf{y}_t := \mathbf{y}(t)$ in stochastic analysis. In particluar, we are interested in the optimal control for a time homogeneous Markov process and the terminal time being the stopping time when the SDE solution hits some closed set B, i.e., $\tau := \inf\{t \geq 0; \mathbf{y}_t \in \bar{B}\}$. In this case, the terminal cost function g is also called the boundary cost function, to be specific, in Theorem 3.3.

Given initial probability measure μ_0 on $\mathcal{N}$ concentrating on the local minimum a of the potential U, consider the stochastic optimal control problem in the infinite time horizon with running cost function $\frac{1}{2}|\mathbf{v}_t|^2$ and boundary cost function $g(\mathbf{y}_\tau)$,

$$(2.4) \quad \begin{aligned} &\gamma = \inf_{\mathbf{v}} \mathbb{E} \left\{ \int_0^\tau \tfrac{1}{2} |\mathbf{v}_t|^2 \, dt + \chi_{\tau < \infty} g(\mathbf{y}_\tau) \right\} \\ &\text{s.t. } d\mathbf{y}_t = (-\nabla U(\mathbf{y}_t) + \mathbf{v}_t) \, dt + \sqrt{2\varepsilon} \, d_{\mathcal{N}} B_t, \quad t \in (0, \tau), \qquad \mathbf{y}_t|_{t=0} \sim \mu_0. \end{aligned}$$

Here χ is the indicator function, $|\mathbf{v}|$ is the Euclidean length of $\mathbf{v}$ in $\mathbb{R}^\ell$, and $d_{\mathcal{N}} B_t$ is shorthand notation for the Brownian motion on manifold $\mathcal{N}$ in the sense of (1.1), which will be used in the following context. In Nelson's theory of stochastic mechanics, $\mathbf{v}$ can be regarded as an average velocity, and the running cost function $L = \frac{1}{2}|\mathbf{v}|^2$ is the classical action integrand including only kinetic energy. The obtained optimal control $\mathbf{v}_t = \mathbf{v}(\mathbf{y}_t)$ is a feedback control and is called the stationary Markov control policy. Since the original Markov process is on a closed manifold $\mathcal{N}$ and U is smooth enough so that the drift vector is bounded continuous on $\mathcal{N}$, we will always have the positive recurrence property provided the landscape is continuous. From now on, we focus on the case $\tau < \infty$, a.s. We remark that practical problems often have dynamics mainly concentrated on a closed manifold due to equality and inequality constraints between different components of variables—for instance the alanine dipeptide example in section 6. So in this paper we only limit ourselves to the case that $\mathcal{N}$ is a closed manifold.

With the small parameter ε, recall that the original Markov process Y_t on manifold $\mathcal{N}$ without control has the corresponding generator $Qf = \varepsilon \Delta f - \nabla U \cdot \nabla f$. The control $\mathbf{v}$ in the stochastic control problem (2.4) can be regarded as an additional driven force to the original Markov process. For the deterministic optimal control case $\varepsilon \to 0$, (2.4)

is closely related to the least action problem (2.2) in an infinite time horizon, which is also known as Peierls barrier (or Mañé potential if a is not steady state). We refer the reader to [GL22b] for discussions on the exchanging limits $\varepsilon \to 0$, $T \to +\infty$ and for connections with weak KAM solutions to the corresponding Hamilton–Jacobi equation.

3. Optimal control viewpoint for the transition path theory for the continuous Markov process. In this section, the main goal is to give a stochastic optimal control interpretation for the transition path theory. We will first review the transition path theory in section 3.1. Then in section 3.2, we prove that the committor function in the transition path theory leads to a stochastic optimal control with which the controlled Markov process realizes the transitions from A to B almost surely.

3.1. Review of the transition path theory. Now we review and explain some concepts in the transition path theory including the committor function, the effective transition path process, and the density/current of transition paths; see original work [EVE06].

3.1.1. Committor function. We start from the original Markov process Y_t with generator

$$(3.1) \qquad Qf = \varepsilon \Delta f - \nabla U \cdot \nabla f.$$

Let A and B be two disjoint absorbing sets of attractors a, b. To study the conditioned process with the conditions on paths starting from A then ending in B, one should find an appropriate excessive function q and calculate the transition probabilities of the conditioned process by using Doob h-transform via q.

Remark 3.1. As mentioned in section 2.2, we know that the SDE solution Y_t hits $\overline{A \cup B}$ at a finite time due to the positive recurrence of the process Y_t on the closed manifold $\mathcal{N}$. For an unbounded domain, the recurrence can be ensured by some specific condition. For instance, we assume that there exists $R_0 > 0$ such that for any $r > R_0$,

$$(3.2) \qquad \nabla_\mathbf{n} U \Big|_{|\mathbf{y}|=r} > \frac{c}{r} \quad \text{for some constant } c > \varepsilon d + 1.$$

Here d is the dimension of manifold $\mathcal{N}$. Here $|\mathbf{y}| = r$ is the geodesic ball on $\mathcal{N}$ and $\mathbf{n} \in T_\mathcal{N}$ is the outer normal vector of the ball. Consequently, $\frac{|\mathbf{y}|^2}{2}$ is a Lyapunov function such that

$$Q\left(\frac{|\mathbf{y}|^2}{2}\right) = \varepsilon d - \nabla U \cdot \mathbf{y} \le -1 \quad \text{for } |\mathbf{y}| > R_0.$$

Applying [BKRS15, Corllaries 2.4.2 and 2.4.3] with this Lyapunov function, we know that condition (3.2) ensures the existence of an invariant measure for process Y_t. This invariant measure is also unique by [BKRS15, Theorem 4.1.6]. Using the same Lyapunov function as in [Kha12, Theorem 3.9] (see also [Ver97, Theorem 3]), we find that condition (3.2) also ensures the positive recurrence in $\mathbb{R}^d$.

Define the stopping time $\tau_B := \inf\{t \ge 0; Y_t \in \bar{B}\}$ (resp., τ_A) of process Y_t when it hits B (resp., A). The probability for the paths hitting B before A is given by the forward committor function $q(\mathbf{y})$, a.k.a. harmonic potential, which is the solution of

$$(3.3) \qquad Qq(\mathbf{y}) = 0, \quad \mathbf{y} \in (\overline{A \cup B})^c,$$

with the Dirichlet boundary conditions

$$(3.4) \qquad q(\mathbf{y}) = 0, \, \mathbf{y} \in \bar{A}, \qquad q(\mathbf{y}) = 1, \, \mathbf{y} \in \bar{B}.$$

LEMMA 3.2. *The solution $q(\mathbf{y})$ to (3.3) with (3.4) satisfies $0 < q(\mathbf{y}) < 1$, $\mathbf{y} \in \overline{(A \cup B)}^c$.*

Proof. Since $\mathcal{N}$ is a closed manifold, $U(\mathbf{y})$ smooth enough, and $\bar{A} \cap \bar{B} = \emptyset$, there exists a solution $q(\mathbf{y}) \in C^2((\overline{A \cup B})^c) \cap C(\overline{A^c \cap B^c})$ to (3.3) with (3.4). Then by the strong maximum principle, we conclude that $0 < q(\mathbf{y}) < 1$, $\mathbf{y} \in \overline{(A \cup B)}^c$. $\qquad \square$

As an important consequence, the density and the current of transition paths can be calculated using the committor function; see the detailed revisit in section 3.1.3.

3.1.2. Generator for the conditioned process. To describe the conditioned process with the conditions that paths start from A and then end in B, [LN15] characterized the selection of the reactive paths coming from A and then hitting B by using the probability measure on the path space such that $\tau_A > \tau_B$.

The associated conditioned process, called the transition path process, is denoted as Z_t. For $Z_0 = \mathbf{y}_0 \in \overline{(A \cup B)}^c$, the generator of this conditioned process Z_t can be described using the Doob h-transform. Precisely, using committor function q as the excessive function and by the Doob h-transform, the generator for conditioned process Z_t is

$$(3.5) \qquad Q^q f = \frac{1}{q} Q(qf) = Qf + \frac{2\varepsilon \nabla q}{q} \cdot \nabla f.$$

Since $q = 0$ in $\bar{A}$, a singular drift term prevents Z_t from hitting A and also pushes $Z_t \in \partial A$ into $\overline{(A \cup B)}^c$. For the delicate case Z_0 starting from ∂A with an appropriate initial law on ∂A, [LN15, Theorem 1.2] proved that the conditioned process Z_t with the augmented filtration is same in law as the kth transition path process exiting from A and then hitting B defined in [EVE06, MSVE06, EVE10]. Here kth path means a generic path exiting from A at the kth time for some generic k; see [LN15, (1.5)]. More precisely, the initial and end distribution for Z_t, a.k.a. reactive exit, and entrance distribution ν_0, ν_1, can be calculated by the Dirichlet to Neumann map of the elliptic equation for committor function (3.3) [LN15, Proposition 1.5].

In section 3.2, we will prove the resulting conditioned process (the transition path process) Z_t can be regarded as the original process with an additional control $\mathbf{v} = \frac{2\varepsilon \nabla q}{q}$. This control, indeed optimal control, together with the original landscape U, leads to an effective potential $U^e := U - 2\varepsilon \ln q$, which is $+\infty$ for $\mathbf{y} \in \bar{A}$ and U for $\mathbf{y} \in \bar{B}$. This effective potential guides the associated SDE of $\tilde{Y}_t$ to the absorbing set B before hitting A.

3.1.3. Density and current of transition paths. Next, using the conditioned process Z_t, which is also the controlled process $\tilde{Y}_t$ in (3.20), and its generator Q^q, we sketch the derivation of the current of transition paths. Recall that the equilibrium density of the original Markov process Y_t is $\pi \propto e^{-\frac{U}{\varepsilon}}$. From [LN15, Proposition 1.9] and [EVE06, Proposition 2], the density of transition paths is

$$(3.6) \qquad \rho^R(\mathbf{y}) = \pi(\mathbf{y}) q(\mathbf{y}) (1 - q(\mathbf{y})).$$

Then some elementary calculations show that

$$(3.7) \qquad (Q^q)^* \rho^R(\mathbf{y}) = 0, \quad \mathbf{y} \in \overline{(A \cup B)}^c.$$

From (3.5) and (3.1),

$$(3.8) \qquad 0 = (Q^q)^* \rho^R = Q^* \rho^R - \nabla \cdot \left(\rho^R \frac{2\varepsilon \nabla q}{q} \right) = \varepsilon \nabla \cdot \left(\pi \nabla \frac{\rho^R}{\pi} - \rho^R \frac{2\nabla q}{q} \right).$$

This divergence form, together with (3.6), gives the current of transition paths from A to B (up to a factor ε)

$$(3.9) \qquad J_R := -\pi \nabla \frac{\rho^R}{\pi} + \rho^R \frac{2\nabla q}{q} = -\pi \nabla [q(1-q)] + 2\pi(1-q)\nabla q = \pi \nabla q.$$

One can directly verify that there is an equilibrium such that

$$(3.10) \qquad (Q^q)^* \pi^e = 0, \qquad \pi^e := e^{-\frac{U^e}{\varepsilon}} = \pi q^2,$$

which vanishes at A. However, we point out ρ^R is not an equilibrium for the controlled process, although $(Q^q)^* \rho^R = 0$ inside $(\overline{A \cup B})^c$. Notice that $\rho^R = 0$ vanishes at both $\bar{A}$ and $\bar{B}$, while π^e only vanishes at $\bar{B}$. That is to say, only π^e is the equilibrium for the controlled process, which prevents the particle from hitting on A but drives it to B. With different boundary conditions, ρ^R and π^e are completely different. We will discuss details of ρ^R and π^e for the discrete case in section 4.2.2.

3.2. Stochastic optimal control interpretation of the committor function. In this subsection, we will prove that the committor function q gives a stochastic optimal control such that the controlled Markov process realizes the transition from A to B with minimum running and terminal cost. We will first illustrate the idea of optimal change of measure in an abstract measurable space and then prove the stochastic optimal control interpretation in Theorem 3.3.

3.2.1. Duality between the relative entropy and the Helmholtz free energy. It is well known that the canonical ensemble is closely related to the optimal change of measure for the Helmholtz free energy. More precisely, let $(\Omega, \mathcal{F})$ be a measurable space, and let $\mathbb{P}(\Omega)$ be the family of probability measures on Ω. Denote Hamiltonian $H \in \mathbb{R}$ as a measurable function on Ω. For a reference measure (a.k.a. prior measure) $P \in \mathbb{P}(\Omega)$ and any $\beta > 0$, we define the Helmholtz free energy of Hamiltonian H with respect to P as

$$(3.11) \qquad F(H) := -\frac{1}{\beta} \ln \left(\int_\Omega e^{-\beta H(\omega)} \, dP(\omega) \right) \in [-\infty, +\infty).$$

For any other measure $\tilde{P} \in \mathbb{P}(\Omega)$ which is absolutely continuous with respect to P, denote by $\mathrm{KL}(\tilde{P}||P) = \int_\Omega \ln(\frac{d\tilde{P}}{dP}) \, d\tilde{P}$ the relative entropy with respect to P. Then we have the following Legendre-type transformations (Donsker and Varadhan's variational formula) and duality in statistical mechanics; cf. [DS01].

(i) For any measure $\tilde{P} \ll P$

$$(3.12) \qquad -\frac{1}{\beta} \mathrm{KL}(\tilde{P}||P) = \sup_H \left\{ \int_\Omega H(\omega) \, d\tilde{P}(\omega) - F(H) \right\};$$

(ii) for any bounded function $H(\omega)$

$$
\begin{aligned}
(3.13) \qquad F(H) &= \inf_{\tilde{P} \ll P} \left\{ \int_\Omega H(\omega) \, d\tilde{P}(\omega) + \frac{1}{\beta} \mathrm{KL}(\tilde{P}||P) \right\} \\
&= \inf_{\tilde{P} \ll P} \left\{ \int_\Omega \left(H(\omega) + \frac{1}{\beta} \ln \frac{d\tilde{P}(\omega)}{dP(\omega)} \right) d\tilde{P}(\omega) \right\}.
\end{aligned}
$$

In Theorem 3.3 later, we will see the second Legendre-type transformation (ii) is still true for a Hamiltonian g defined in (3.25), and we use it for probability measures (induced by coordinate processes) on path space $\Omega = C([0, +\infty); \mathcal{N})$ to prove the optimality. To show the idea of the proof, if $dP = \rho_0\, dx$ and $d\tilde{P} = \rho\, dx$, the optimal density ρ^* in the transformation is achieved when

$$(3.14) \qquad e^{-\beta H - 1 + \lambda} = \frac{\rho^*}{\rho_0}, \qquad \int \rho^* = 1 = e^{\lambda - 1} \int e^{-\beta H} \rho_0\, dx,$$

where λ is the Lagrange multiplier to ensure ρ is a probability density. Then we have

$$(3.15) \qquad \int H \rho^*\, dx + \frac{1}{\beta} \int \ln \frac{\rho^*}{\rho_0}\, \rho^*\, dx = \frac{\lambda - 1}{\beta} = F(H).$$

3.2.2. Committor function gives the optimal control in infinite time horizon. In general, given an arbitrary control field in the gradient form, $\mathbf{v} = 2\varepsilon \nabla \ln h$ for some function h, the generator for the controlled process is not exactly the Doob h-transform. Indeed, by Ito's formula, the generator under the control $\mathbf{v}$ is

$$(3.16) \qquad Q^h = Q + \mathbf{v} \cdot \nabla = Q + 2\varepsilon \nabla \ln h \cdot \nabla.$$

On the other hand, by elementary calculations, the Doob h-transform satisfies the identity

$$(3.17) \qquad \frac{1}{h} Q(hf) = Qf + f \frac{Qh}{h} + 2\varepsilon \nabla \ln h \cdot \nabla f = Q^h f + f \frac{Qh}{h}$$

for any test function f. We can recast the controlled generator Q^h as

$$(3.18) \qquad Q^h f = \frac{1}{h} Q(hf) - f \frac{Qh}{h}.$$

Now we give a theorem on the optimality of the control $\mathbf{v} = \frac{2\varepsilon \nabla q}{q} = 2\varepsilon \nabla \ln q$ in an infinite time stochastic optimal control problem, where q is the committor function solving (3.3) with boundary condition (3.4). As a consequence of the optimal control $\mathbf{v} = 2\varepsilon \nabla \ln q$, we recover $\frac{1}{q} Q(qf) = Q^q f$.

From the stochastic optimal control viewpoint, a control should drive the process from A to B with minimum cost. To prevent Y_t hitting on A, we choose the terminal cost as

$$g(x) := \begin{cases} +\infty & \text{in } \bar{A}, \\ 0 & \text{in } \bar{B}. \end{cases}$$

However, to avoid the difficulty that an unbounded terminal cost leads to an unbounded stopping time τ_A, we use a regularization method as below. We first define a cut-off terminal cost

$$(3.19) \qquad g_{\mathrm{N}}(x) := \begin{cases} N, & \text{in } \bar{A}, \\ 0, & \text{in } \bar{B}, \end{cases}$$

where $N \gg 1$. Then we prove the following theorem to state that the regularized committor function satisfying (3.22) and (3.23) gives the optimal control with the cut-off terminal cost (3.19). In the next section, we prove the monotone dependence of the committor function and the associated value function on the cut-off number N. And then taking $N \to +\infty$, the limit $q(\mathbf{y}) = \lim_{N \to +\infty} g_N(\mathbf{y})$ recovers the committor function and $\frac{1}{q} Q(qf) = Q^q f$.

THEOREM 3.3. *Assume the original Markov process Y_t has generator $Qf = \varepsilon \Delta f - \nabla U \cdot \nabla f$, $\varepsilon > 0$. The forward commitor function $q_{\rm N}$ in (3.22) gives an optimal control $\mathbf{v}_{\rm N}^* = \frac{2\varepsilon \nabla q_{\rm N}}{q_{\rm N}}$ in the sense that it drives the controlled process $\tilde{Y}_t$ starting from $\boldsymbol{y} \in (\overline{A \cup B})^c$ to the set B before hitting A with the least action*

$$
\begin{aligned}
(3.20) \qquad \gamma_{\rm N}(\boldsymbol{y}) := &\min_{\mathbf{v}_{\rm N} \in \mathcal{A}_{\rm N}} \mathbb{E}_P \left[\int_0^\tau \frac{1}{2} |\mathbf{v}_{\rm N}(\tilde{Y}_s)|^2 \, \mathrm{d}s + g_{\rm N}(\tilde{Y}_\tau) \right] \\
&s.t. \quad \mathrm{d}\tilde{Y}_t = (-\nabla U(\tilde{Y}_t) + \mathbf{v}_{\rm N}(\tilde{Y}_t)) \, \mathrm{d}t + \sqrt{2\varepsilon} \, \mathrm{d}_{\mathcal{N}} B_t, \ \tilde{Y}_0 = \boldsymbol{y},
\end{aligned}
$$

where $\tau := \inf\{t \geq 0; \tilde{Y}_t \in \overline{A \cup B}\}$ is the stopping time, and the admissible control belongs to

$$
(3.21) \qquad \mathcal{A}_{\rm N} := \left\{ \mathbf{v}_{\rm N} \in T_{\mathcal{N}}; \ \mathbb{E}_P \left(e^{\int_0^\tau \frac{1}{4\varepsilon} |\mathbf{v}_{\rm N}(\tilde{Y}_s)|^2 \, \mathrm{d}s} \right) < \infty \right\},
$$

where $T_{\mathcal{N}}$ is C^1 tangent vector field on $\mathcal{N}$. Moreover, $\gamma_{\rm N}(\mathbf{y}) = -2\varepsilon \ln q_{\rm N}(\mathbf{y})$ and the optimal control $\mathbf{v}_{\rm N}^*$ leads to an effective potential $U^e := U - 2\varepsilon \ln q_{\rm N}$ for the controlled Markov process $\tilde{Y}_t$ with the generator $Q^{q_{\rm N}}$ defined in (3.5), and the corresponding effective potential is $\pi_{\rm N}^e = \pi q_{\rm N}^2$.

Proof. Choose $\Omega = C([0, +\infty); \mathcal{N})$, with the product σ-algebra, as our measurable space [Var07]. Any element $\mathbf{y} \in \Omega$ gives a coordinate process $Y_t(\mathbf{y}) := \mathbf{y}(t) \in \mathcal{N}$, $t \geq 0$.

First, recall that for a closed manifold, the stopping time $\tau := \inf\{t \geq 0; Y_t \in \overline{A \cup B}\} < \infty$, a.s. Define a regularized committor function $q_{\rm N}$ satisfying

$$
(3.22) \qquad Q q_{\rm N}(\mathbf{y}) = 0, \quad \mathbf{y} \in (\overline{A \cup B})^c,
$$

with the Dirichlet boundary conditions

$$
(3.23) \qquad q_{\rm N}(\mathbf{y}) = e^{-\beta N}, \, \mathbf{y} \in \bar{A}, \qquad q_{\rm N}(\mathbf{y}) = 1, \, \mathbf{y} \in \bar{B}.
$$

From [Eva13, section 6.2.1], the stochastic characterization of $q_{\rm N}$ can be expressed as

$$
(3.24) \qquad q_{\rm N}(\boldsymbol{y}) = \mathbb{E}_P(f_{\rm N}(Y_\tau)), \quad \boldsymbol{y} \in \overline{A \cup B}^c,
$$

with function $f_{\rm N}(\mathbf{z})$ on $\overline{A \cup B}$, $f_{\rm N} = e^{-\beta N}$, $\mathbf{z} \in \bar{A}$, while $f_{\rm N} = 1$, $\mathbf{z} \in \bar{B}$. Here the expectation is taken under the probability measure P (called the reference measure) on the path space Ω associated with all realizations of the original SDE of Y_t starting from $\boldsymbol{y} \in (\overline{A \cup B})^c$. Define $\beta := \frac{1}{2\varepsilon}$ and function

$$
(3.25) \qquad g_{\rm N}(x) = -\frac{1}{\beta} \ln f_{\rm N} = \left\{ \begin{array}{ll} N & \text{in } \bar{A}; \\ 0 & \text{in } \bar{B}. \end{array} \right.
$$

Then choose Hamiltonian $H(\mathbf{y}) := g_{\rm N}(Y_\tau(\mathbf{y}))$ for $\mathbf{y} \in \Omega$. Since the original SDE for Y_t is translation invariant with respect to time (stationary with respect to time), the feedback control function $\mathbf{v}_{\rm N}(Y_t)$ (stationary Markov control) does not explicitly depend on t and we can take the starting time as $t = 0$ without loss of generality. We consider the optimal control problem (3.20) with the admissible control in $\mathcal{A}_{\rm N}$. $\mathcal{A}_{\rm N}$ in (3.21) is the well-known Novikov condition in the Girsanov transformation, which ensures the almost sure positivity of the Radon–Nikodym derivative in (3.27). It is easy to see that $\mathbf{v}_{\rm N} = 0$ belongs to $\mathcal{A}_{\rm N}$ so $\mathcal{A}_{\rm N} \neq \emptyset$. However, from the definition of $g_{\rm N}$, $g_{\rm N}(Y_\tau) = N$ when $Y_\tau \in \bar{A}$, so for large N, $\mathbf{v}_{\rm N} = 0$ is not an optimal control.

Second, we find the minimizer $\gamma_{\rm N}$ (a.k.a. value function) and the corresponding optimal control $\mathbf{v}_{\rm N}^*$. Let $\tilde{P}$ be the probability measure on Ω associated with all

realizations of the SDE of $\tilde{Y}_t$ with control $\mathbf{v}_\mathrm{N}$. By the Girsanov theorem, Y_t is a Brownian motion under measure P, and $\tilde{Y}_t$ is a Brownian motion under measure $\tilde{P}$. As a consequence,

$$(3.26) \qquad \mathbb{E}_P(e^{-\beta g_\mathrm{N}(Y_\tau)}) = \mathbb{E}_{\tilde{P}}(e^{-\beta g_\mathrm{N}(\tilde{Y}_\tau)}) = \mathbb{E}_P\left(e^{-\beta g_\mathrm{N}(\tilde{Y}_\tau)} \frac{\mathrm{d}\tilde{P}}{\mathrm{d}P}\right),$$

where the Radon–Nikodym derivative is given by [Var07, Theorem 6.2]

$$(3.27) \qquad \frac{\mathrm{d}\tilde{P}}{\mathrm{d}P} = e^{-\beta \int_0^\tau \sqrt{2\varepsilon}\mathbf{v}_\mathrm{N}(\tilde{Y}_s)\cdot \mathrm{d}_\mathcal{N}B_s - \frac{\beta}{2}\int_0^\tau |\mathbf{v}_\mathrm{N}(\tilde{Y}_s)|^2\,\mathrm{d}s} > 0, \quad P\text{-a.s.}$$

and the sign in front of $\mathrm{d}_\mathcal{N}B$ is negative following the convention. In short, we have

$$(3.28)$$
$$\mathbb{E}_P(e^{-\beta H(\mathbf{y})}) = \mathbb{E}_P(e^{-\beta g_\mathrm{N}(Y_\tau)}) = \mathbb{E}_P\left(e^{-\beta\left(g_\mathrm{N}(\tilde{Y}_\tau) + \int_0^\tau \sqrt{2\varepsilon}\mathbf{v}_\mathrm{N}(\tilde{Y}_s)\cdot \mathrm{d}_\mathcal{N}B_s + \frac{1}{2}\int_0^\tau |\mathbf{v}_\mathrm{N}(\tilde{Y}_s)|^2\,\mathrm{d}s\right)}\right).$$

Then by Jensen's inequality and (3.26),

$$(3.29) \quad e^{-\beta \mathbb{E}_\mathrm{N}\left(g_\mathrm{N}(\tilde{Y}_\tau) + \int_0^\tau \frac{1}{2}|\mathbf{v}_\mathrm{N}(\tilde{Y}_s)|^2\,\mathrm{d}s\right)} \le \mathbb{E}_P\left(e^{-\beta g_\mathrm{N}(\tilde{Y}_\tau)}\frac{\mathrm{d}\tilde{P}}{\mathrm{d}P}\right) = \mathbb{E}_P(e^{-\beta g_\mathrm{N}(Y_\tau)}).$$

Here the equality is achieved if and only if $g_\mathrm{N}(\tilde{Y}_\tau) + \int_0^\tau \sqrt{2\varepsilon}\mathbf{v}_\mathrm{N}(\tilde{Y}_s)\cdot \mathrm{d}_\mathcal{N}B_s + \int_0^\tau \frac{1}{2}|\mathbf{v}_\mathrm{N}(\tilde{Y}_s)|^2\,\mathrm{d}s$ is deterministic. Using Lemma 3.1 and (3.24), we know that

$$(3.30) \qquad q_\mathrm{N}(\mathbf{y}) = \mathbb{E}_P(f_\mathrm{N}(Y_\tau)) = \mathbb{E}_P(e^{-\beta g_\mathrm{N}(Y_\tau)}) > 0, \quad \mathbf{y} \in (\overline{A \cup B})^c.$$

Thus the RHS of (3.29) is always positive. Taking the logarithm to both sides, we have

$$(3.31) \qquad -\beta\mathbb{E}_P\left(g_\mathrm{N}(\tilde{Y}_\tau) + \int_0^\tau \frac{1}{2}|\mathbf{v}_\mathrm{N}(\tilde{Y}_s)|^2\,\mathrm{d}s\right) \le \ln\left(\mathbb{E}_P\left(e^{-\beta g_\mathrm{N}(\tilde{Y}_\tau)}\frac{\mathrm{d}\tilde{P}}{\mathrm{d}P}\right)\right)$$
$$= \ln\left(\mathbb{E}_P(e^{-\beta g_\mathrm{N}(Y_\tau)})\right).$$

Therefore, we obtain

$$\mathbb{E}_P\left(g_\mathrm{N}(\tilde{Y}_\tau) + \int_0^\tau \frac{1}{2}|\mathbf{v}_\mathrm{N}(\tilde{Y}_s)|^2\,\mathrm{d}s\right) \ge -\frac{1}{\beta}\ln\left(\mathbb{E}_P\left(e^{-\beta g_\mathrm{N}(\tilde{Y}_\tau)}\frac{\mathrm{d}\tilde{P}}{\mathrm{d}P}\right)\right)$$
$$(3.32) \qquad\qquad = -\frac{1}{\beta}\ln\left(\mathbb{E}_P(e^{-\beta g_\mathrm{N}(Y_\tau)})\right),$$

which, together with (3.30), gives

$$(3.33) \qquad \gamma_\mathrm{N}(\mathbf{y}) \ge -\frac{1}{\beta}\ln\left(\mathbb{E}_P(e^{-\beta g_\mathrm{N}(Y_\tau)})\right) = -\frac{1}{\beta}\ln q_\mathrm{N}(\mathbf{y}), \quad \mathbf{y} \in (\overline{A \cup B})^c.$$

Furthermore, the verification theorem [FS06, IV.3, Theorem 5.1] shows that the equality is indeed achieved by the Hopf–Cole transformation

$$(3.34) \qquad\qquad\qquad \gamma_\mathrm{N}(\mathbf{y}) = -\frac{1}{\beta}\ln q_\mathrm{N}(\mathbf{y}).$$

Actually, $\gamma_{\mathrm{N}}(\boldsymbol{y})$ satisfies the Hamilton–Jacobi–Bellman (HJB) equation

$$(3.35) \quad \varepsilon \Delta \gamma_{\mathrm{N}} - \frac{1}{2}|\nabla \gamma_{\mathrm{N}}|^2 - \nabla U \cdot \nabla \gamma_{\mathrm{N}} = 0, \quad \text{in } (\overline{A \cup B})^c, \qquad \gamma_{\mathrm{N}} = g_{\mathrm{N}} \text{ on } \overline{A \cup B}.$$

The associated optimal control (optimal feedback), such that

$$(3.36) \qquad \tilde{H}(\mathbf{y}) := g_{\mathrm{N}}(\tilde{Y}_\tau) + \int_0^\tau \sqrt{2\varepsilon} \mathbf{v}_{\mathrm{N}}^*(\tilde{Y}_s) \cdot \, \mathrm{d}_{\mathcal{N}} B_s + \int_0^\tau \frac{1}{2}|\mathbf{v}_{\mathrm{N}}^*(\tilde{Y}_s)|^2 \, \mathrm{d}s$$

is deterministic, is given by

$$(3.37) \qquad \mathbf{v}_{\mathrm{N}}^* = -\nabla \gamma_{\mathrm{N}} = \frac{1}{\beta} \nabla \ln \mathbb{E}_P \left(e^{-\beta g_{\mathrm{N}}(Y_\tau)} \right) = \frac{1}{\beta} \nabla \ln q_{\mathrm{N}}.$$

Indeed, one can verify this by applying Ito's formula to $\gamma_{\mathrm{N}}(\tilde{Y}_\tau)$,

$$(3.38) \quad \begin{aligned} I :=& \gamma_{\mathrm{N}}(\tilde{Y}_\tau) - \gamma_{\mathrm{N}}(\tilde{Y}_0) \\ =& \int_0^\tau \varepsilon \Delta \gamma_{\mathrm{N}}(\tilde{Y}_s) + (-\nabla U + \mathbf{v}_{\mathrm{N}}^*) \cdot \nabla \gamma_{\mathrm{N}}(\tilde{Y}_s) \, \mathrm{d}s + \sqrt{2\varepsilon} \int_0^\tau \nabla \gamma_{\mathrm{N}} \cdot \, \mathrm{d}_{\mathcal{N}} B_s \\ =& \int_0^\tau \left(\varepsilon \Delta \gamma_{\mathrm{N}} - \nabla U \cdot \nabla \gamma_{\mathrm{N}} - |\nabla \gamma_{\mathrm{N}}|^2 \right) (\tilde{Y}_s) \, \mathrm{d}s + \sqrt{2\varepsilon} \int_0^\tau \nabla \gamma_{\mathrm{N}} \cdot \, \mathrm{d}_{\mathcal{N}} B_s \\ =& -\frac{1}{2} \int_0^\tau |\nabla \gamma_{\mathrm{N}}|^2(\tilde{Y}_s) \, \mathrm{d}s + \sqrt{2\varepsilon} \int_0^\tau \nabla \gamma_{\mathrm{N}} \cdot \, \mathrm{d}_{\mathcal{N}} B_s, \end{aligned}$$

where we used $\mathbf{v}_{\mathrm{N}}^* = -\nabla \gamma_{\mathrm{N}}$ and (3.35). Using $\mathbf{v}_{\mathrm{N}}^* = -\nabla \gamma_{\mathrm{N}}$ again, the last two terms above become

$$(3.39) \quad I = -\frac{1}{2} \int_0^\tau |\mathbf{v}_{\mathrm{N}}^*(\tilde{Y}_s)|^2 \, \mathrm{d}s - \sqrt{2\varepsilon} \int_0^\tau \mathbf{v}_{\mathrm{N}}^*(\tilde{Y}_s) \cdot \, \mathrm{d}_{\mathcal{N}} B_s = g_{\mathrm{N}}(\tilde{Y}_\tau) - \tilde{H}(\mathbf{y}).$$

Using the boundary condition of (3.35), $\gamma_{\mathrm{N}}(\tilde{Y}_\tau) = g_{\mathrm{N}}(\tilde{Y}_\tau)$, and $\tilde{Y}_0 = \mathbf{y}$, we have

$$(3.40) \qquad \tilde{H}(\mathbf{y}) = \gamma_{\mathrm{N}}(\tilde{Y}_0) \text{ is deterministic.}$$

Since the optimality ensures $\tilde{H}$ in (3.36) is deterministic, so from (3.34),

$$\mathbb{E}_P \left(e^{-\beta \tilde{H}} \right) = e^{-\mathbb{E}_P(\beta \tilde{H})} = e^{-\beta \gamma_{\mathrm{N}}(\mathbf{y})} = q_{\mathrm{N}} < +\infty,$$

and thus $\mathbf{v}_{\mathrm{N}}^* \in \mathcal{A}_{\mathrm{N}}$.

Finally, plugging the optimal control $\mathbf{v}_{\mathrm{N}}^* = 2\varepsilon \nabla \ln q_{\mathrm{N}}$ into (3.20) shows that the effective potential for the controlled Markov process $\tilde{Y}_t$ is

$$(3.41) \qquad U_{\mathrm{N}}^e = U - 2\varepsilon \ln q_{\mathrm{N}}.$$

Then by Ito's formula, the master equation for the controlled Markov process $\tilde{Y}_t$ is

$$(3.42) \qquad \partial_t \rho = \varepsilon \nabla \cdot \left(e^{-\frac{U_{\mathrm{N}}^e}{\varepsilon}} \nabla(\rho e^{\frac{U_{\mathrm{N}}^e}{\varepsilon}}) \right) = \varepsilon \nabla \left(\pi_{\mathrm{N}}^e \nabla \frac{\rho}{\pi_{\mathrm{N}}^e} \right).$$

Here $\pi_{\mathrm{N}}^e = \pi q_{\mathrm{N}}^2$ is the effective equilibrium. $\qquad \square$

Remark 3.4. Although we focus on a reversible process defined by SDE (1.1), we remark that Theorem 3.3 still holds for irreversible process with a general drift $\boldsymbol{b}$[1]

---

[1]Under assumptions for existence of a solution, for instance, $\boldsymbol{b}$ is smooth enough and $\boldsymbol{b}(\boldsymbol{y}) \cdot \boldsymbol{y} \leq c(1 + |\boldsymbol{y}|^2)$.

and the generator $\tilde{Q}f = \varepsilon\Delta f + \boldsymbol{b}\cdot\nabla f$. The optimal control will be given by $2\varepsilon\nabla\ln q$ with q being the solution to $\tilde{Q}q = 0$ and (3.4). However, the Fokker–Planck equation for irreversible processes does not have a relative entropy formulation. We refer the reader to [GL21] for a structure preserving numerical scheme for irreversible processes with a general drift field, which can be leveraged to construct an optimally controlled random walk on point clouds for general irreversible processes.

3.2.3. Monotone dependence of committor function on cut-off N. Let $N_1 \le N_2$. Let $\hat{q} = q_{N1} - q_{N2}$ and q_{N1}, q_{N2} be the solution to (3.22) with Dirichlet boundary conditions $q_{N1}(\mathbf{y}) = e^{-\beta N_1}$, $q_{N2}(\mathbf{y}) = e^{-\beta N_2}$ on $\bar{A}$. Then $\hat{q}$ satisfies

$$(3.43) \qquad Q\hat{q}(\mathbf{y}) = 0, \quad \mathbf{y} \in (\overline{A\cup B})^c,$$

$$(3.44) \qquad \hat{q}(\mathbf{y}) = e^{-\beta N_1} - e^{-\beta N_2} \ge 0, \mathbf{y} \in \bar{A}, \qquad \hat{q}(\mathbf{y}) = 0, \mathbf{y} \in \bar{B}.$$

Then by the strong maximum principle, $\hat{q} \ge 0$ and thus $q_{N1} \ge q_{N2}$. Knowing this, together with Lemma 3.1, we know that $q_N \ge 0$ and is decreasing with respec to N. Taking the limit $q(\mathbf{y}) := \lim_N q_N(\mathbf{y})$, we see that $q(\mathbf{y})$ satisfies the original committor function (3.3). By using the Hopf–Cole transformation $\gamma(\mathbf{y}) = -\frac{1}{\beta}\ln q(\mathbf{y})$, we obtain that γ satisfies the limiting Hamilton–Jacobi equation

$$(3.45) \quad \varepsilon\Delta\gamma - \frac{1}{2}|\nabla\gamma|^2 - \nabla U\cdot\nabla\gamma = 0 \ \text{ in } (\overline{A\cup B})^c, \qquad \gamma = \left\{ \begin{array}{ll} +\infty & \text{in } \bar{A}, \\ 0 & \text{in } \bar{B}. \end{array} \right.$$

Notice that $\gamma_N(\mathbf{y}) = -\frac{1}{\beta}\ln q_N(\mathbf{y})$ is an increasing function of N. We have $\gamma(\mathbf{y}) = \lim_{N\to+\infty}\gamma_N(\mathbf{y})$. Meanwhile, the limiting effective potential is given by

$$(3.46) \qquad U^e = \lim_{N\to+\infty}(U - 2\varepsilon\ln q_N) = U - 2\varepsilon\ln q.$$

Thus the limiting effective equilibrium is $\pi^e = \pi q^2$.

In summary, the committor function can be regarded as a limit of q_N, which gives the optimal control with cut-off $\mathbf{v}_N^* = 2\varepsilon\nabla\ln q_N$. The corresponding effective potential π^e is given by the limit $\pi^e = \pi q^2$. Numerically, because the singular transition layer in ∇q, we indeed only use the effective equilibrium $\pi^e = \pi q^2$ to construct an optimally controlled random walk on point clouds.

Remark 3.5. Notice that the value function $\gamma(\boldsymbol{y}) = -2\varepsilon\ln q(\boldsymbol{y})$ satisfies

$$(3.47) \qquad 0 = \varepsilon\Delta\gamma - \frac{1}{2}|\nabla\gamma|^2 - \nabla U\cdot\nabla\gamma = -e^{\frac{\gamma}{2\varepsilon}}Q(e^{-\frac{\gamma}{2\varepsilon}}).$$

We comment on the connection with the logarithmic transformation framework developed by Sheu and Fleming [She85], [FS06, section VI]. Define a Hamiltonian operator $Hf := e^f Q(e^{-f})$; then by [FS06, Lemma 9.1, p. 257]

$$(3.48) \qquad Hf = \min_h \left\{ -Q^h f - Q^h(\ln h) + \frac{Qh}{h} \right\}.$$

This Hamiltonian operator and the associated HJB equation for the optimal control for exit problem has been studied in [BH16]. In particular, the authors applied the optimal control verification theorem in [FS06, section VI] to the exit problem in the infinite time horizon and constructed an optimally controlled Markov chain based on the solution to the associated HJB equation.

Remark 3.6. We remark that Theorem 3.3 uses a terminal cost function g and the associated committor function q to construct an optimal feedback $\mathbf{v}^*$ and thus the associated controlled process $\tilde{Y}$. More importantly, the transition from absorbing set A to another absorbing set B is a rare event for the original Markov process Y_t while this transition becomes an almost sure event for the controlled Markov process $\tilde{Y}_t$. This has a significant statistical advantage because it uses the controlled process $\tilde{Y}_t$, which realizes the conformational transitions almost surely. The computations for statistic quantities in the original rare event become more efficient; see Algorithm 1 for the controlled random walk on point clouds.

4. Markov chain and transition path theory on point clouds. This section focuses on constructing an approximated Markov chain on point clouds and computing the discrete analogies in the transition path theory on point clouds. In section 4.1, we will first introduce a finite volume scheme which approximates the original Langevin dynamics (1.1) and its master equation on $\mathcal{N}$. In section 4.2, based on the approximated Markov chain, we design the discrete counterparts for the committor functions, the discrete Doob h-transform, and the generator for the optimal controlled Markov chain in the transition path theory on point clouds.

4.1. Finite volume scheme and the approximated Markov chain on point clouds. In this section, we first propose a finite volume scheme for the original Fokker–Planck equation based on a data-driven approximated Voronoi tesselation for $\mathcal{N}$. Then we reformulate it as a Markov process on point clouds.

4.1.1. Voronoi tesselation and finite volume scheme. Suppose $(\mathcal{N}, d_{\mathcal{N}})$ is a d dimensional smooth closed submanifold of $\mathbb{R}^{\ell}$ and $d_{\mathcal{N}}$ is induced by the Euclidean metric in $\mathbb{R}^{\ell}$. $D := \{\mathbf{y}_i\}_{i=1:n}$ is a point cloud sampled from some density on $\mathcal{N}$ bounded below and above. It is proved that the data points D are well distributed on $\mathcal{N}$ whenever the points are sampled from a density function with lower and upper bounds [TS15, LLL19]. Define the Voronoi cell as

(4.1)
$$C_i := \{\mathbf{y} \in \mathcal{N};\ d_{\mathcal{N}}(\mathbf{y}, \mathbf{y}_i) \leq d_{\mathcal{N}}(\mathbf{y}, \mathbf{y}_j) \text{ for all } \mathbf{y}_j \in D\} \quad \text{with volume } |C_i| = \mathcal{H}^d(C_i).$$

Then $\mathcal{N} = \cup_{i=1}^n C_i$ is a Voronoi tessellation of $\mathcal{N}$. Denote the Voronoi face for cell C_i as

(4.2)
$$\Gamma_{ij} := C_i \cap C_j \text{ with its area } |\Gamma_{ij}| = \mathcal{H}^{d-1}(\Gamma_{ij})$$

for any $j = 1, \ldots, n$. If $\Gamma_{ij} = \emptyset$ or $i = j$, then we set $|\Gamma_{ij}| = 0$. Define the associated adjacent sample points as

(4.3)
$$\text{VF}(i) := \{j;\ \Gamma_{ij} \neq \emptyset\}.$$

By Ito's formula, SDE (1.1) gives the following Fokker–Planck equation, which is the master equation for the density $\rho(\mathbf{y})$ in terms of $\mathbf{y}$,

(4.4)
$$\partial_t \rho = \nabla \cdot (\varepsilon \nabla \rho + \rho \nabla U) =: \text{FP}^{\mathcal{N}} \rho.$$

Denote the equilibrium $\pi := e^{-\frac{U}{\varepsilon}}$. The Fokker–Planck operator has the following equivalent form:

(4.5)
$$\begin{aligned} \text{FP}^{\mathcal{N}}(\rho) &= \varepsilon \Delta \rho + \nabla \cdot (\rho \nabla U) = \nabla \cdot (\rho (\varepsilon \nabla \ln \rho + \nabla U)) \\ &= \varepsilon \nabla \cdot \left(\rho \nabla \ln \frac{\rho}{\pi} \right) = \varepsilon \nabla \cdot \left(\pi \nabla \frac{\rho}{\pi} \right). \end{aligned}$$

Using (4.5), we have the following finite volume scheme:

$$(4.6) \qquad \frac{\mathrm{d}}{\mathrm{d}t}\rho_i|C_i| = \sum_{j\in\mathrm{VF}(i)} \frac{\pi_i+\pi_j}{2|y_i-y_j|}|\Gamma_{ij}|\left(\frac{\rho_j}{\pi_j}-\frac{\rho_i}{\pi_i}\right), \quad i=1,\dots,n,$$

where π_i is the approximated equilibrium density at $\mathbf{y}_i$ with the volume element $|C_i|$. One can also recast (4.6) as a backward equation formulation:

$$(4.7) \qquad \frac{\mathrm{d}}{\mathrm{d}t}\frac{\rho_i}{\pi_i} = \sum_{j\in\mathrm{VF}(i)} \frac{\pi_i+\pi_j}{2\pi_i|C_i||y_i-y_j|}|\Gamma_{ij}|\left(\frac{\rho_j}{\pi_j}-\frac{\rho_i}{\pi_i}\right), \quad i=1,\dots,n.$$

Define a Q-matrix

$$(4.8) \qquad Q_{ij} = \frac{\pi_i+\pi_j}{2\pi_i|C_i||y_i-y_j|}|\Gamma_{ij}| \geq 0, \quad j\neq i, \qquad Q_{ii} = -\sum_{j\neq i}Q_{ij}.$$

Notice that row sums zero, $\sum_j Q_{ij} = 0$. Then Q is the generator of the associated Markov process. We rewrite (4.7) in the matrix form

$$(4.9) \qquad \frac{\mathrm{d}}{\mathrm{d}t}\frac{\rho}{\pi} = Q\frac{\rho}{\pi} \qquad \text{with } \frac{\rho}{\pi} = \left(\frac{\rho_i}{\pi_i}\right)_{i=1:n}.$$

With an adjoint Q-matrix, (4.6) can also be recast in matrix form:

$$(4.10) \qquad \frac{\mathrm{d}}{\mathrm{d}t}\rho|C| = Q^*(\rho|C|) \qquad \text{with } \rho|C| = \{\rho_i|C_i|\}_{i=1:n}.$$

In practice, since we don't have the exact manifold information, the volume of the Voronoi cells C_k and the area of the Voronoi faces Γ_{kl} need to be approximated. We refer the reader to [GLW20, Algorithm 1] for the algorithm for approximating $|C_k|$ and $|\Gamma_{ij}|$ and the convergence analysis of this solver (4.6) for the Fokker–Planck equation (4.4). We denote the approximated volumes as $|\tilde{C}_k|$ and the approximated areas as $|\tilde{\Gamma}_{kl}|$. After replacing $|C_k|$ by the approximated volumes $|\tilde{C}_k|$ and replacing $|\Gamma_{kl}|$ by the approximated areas $|\tilde{\Gamma}_{kl}|$, (4.6)/(4.12) becomes an approximated Markov process on point clouds, which is an implementable solver for the Fokker–Planck equation on $\mathcal{N}$. We drop tildes when there is no confusion in the following contexts.

The [GLW20, Lemma 3.10] shows that under the assumption that each Voronoi cell is contained in a small ball centered at a certain data point, the algorithm can make a correct approximation of $|C_k|$ and $|\Gamma_{ij}|$. This assumption means the data cloud is dense enough on the manifold $\mathcal{N}$. When the data is not enough, we can use some data-enrichment techniques to sample more data on the manifold to assist the estimation. We will show an example for this procedure in numerical Example 3.

4.1.2. Markov process on point clouds. With the approximated volumes $|C_i|$ and the approximated areas $|\Gamma_{ij}|$, one can interpret the finite volume scheme (4.6) as the forward equation for a Markov process with transition probability matrix (P_{ji}) (from j to i) and diagonal rate matrix $R = \mathrm{diag}(\lambda_j)$. Here P and R are determined by Q-matrix as follows:

$$\lambda_i := \sum_{j\neq i}Q_{ij} = \frac{1}{2|C_i|\pi_i}\sum_{j\in\mathrm{VF}(i)}\frac{\pi_i+\pi_j}{|y_i-y_j|}|\Gamma_{ij}|, \quad i=1,2,\dots,n;$$

$$(4.11) \qquad P_{ij} := \begin{cases} \dfrac{Q_{ij}}{\lambda_i} = \dfrac{1}{\lambda_i}\dfrac{\pi_i+\pi_j}{2\pi_i|C_i|}\dfrac{|\Gamma_{ij}|}{|y_i-y_j|}, & j\in\mathrm{VF}(i); \\[2ex] 0, & j\notin\mathrm{VF}(i). \end{cases}$$

Assume that $\pi_i > 0$ for all i; then we have $\lambda_i > 0$ for all i. One can see P has nonnegative entries and satisfies row sum one $\sum_i P_{ji} = 1$. In the matrix form, we have $Q = R(P - I)$. Then the finite volume scheme (4.6) can be recast as

$$(4.12) \qquad \frac{\mathrm{d}}{\mathrm{d}t}\rho_i|C_i| = \sum_{j\in\mathrm{VF}(i)} \lambda_j P_{ji}\rho_j|C_j| - \lambda_i\rho_i|C_i|, \quad i = 1, 2, \ldots, n,$$

and the detailed balance property

$$(4.13) \qquad Q_{ji}\pi_j|C_j| = P_{ji}\lambda_j\pi_j|C_j| = P_{ij}\lambda_i\pi_i|C_i| = Q_{ij}\pi_i|C_i|.$$

4.2. Committor function, currents, and controlled Markov chain on point clouds. In this section, we first review the corresponding concepts for the transition path theory on point clouds. Then from the optimal control viewpoint, we construct a finite volume scheme for the controlled Fokker–Planck equation and the associated controlled Markov process (random walk on point clouds).

4.2.1. Committor function, currents, and transition rate. Suppose the local minima a and b of U are two cell centers with indices i_a and i_b. Below, we clarify the discrete counterparts of section 3.1 for committor functions q, the density of transition paths ρ^R, the current of transition paths J_R, and the transition rates k_{AB}.

First, from the backward equation formulation (4.7), the forward committor function q_i, $i = 1, \ldots, n$, from a to b satisfies

$$(4.14) \qquad \sum_{j\in VF(i)} Q_{ij}(q_j - q_i) = 0, \quad i \neq i_a, i_b,$$

$$q_{i_a} = 0, \quad q_{i_b} = 1.$$

Note that we only solve the committor function for a discrete Markov process by solving a linear system. The Q-matrix is directly obtained from the approximated transition probability and jumping rate computed from data point probing the manifold; see (4.8). With the Q-matrix, the cost of solving this linear system only depends on the number of sample points. Whether there are enough data point probing the manifold is a static geometric problem, rather than a dynamic sampling issue. As long as there are well-distributed data points probing the manifold, the diffusion tensor on the manifold is automatically embedded in the Markov chain constructed from those data points.

Second, the discrete density of the reactive paths [MSVE09, Remark 2.10] is defined as

$$(4.15) \qquad \rho_i^R := \pi_i q_i(1 - q_i).$$

Third, with the constructed Q-matrix in (4.8), the current from site i to site j of the reactive path from state a to state b is given by [MSVE09, Remark 2.17]

$$(4.16) \qquad J_{ij}^R := Q_{ij}\pi_i(q_j - q_i) = \frac{(\pi_i + \pi_j)|\Gamma_{ij}|}{2} \frac{q_j - q_i}{|y_i - y_j|},$$

which is the counterpart of the current in (3.9). Due to (4.14), it is easy to check the current is divergence free, i.e., satisfying the Kirchhoff current law,

$$(4.17) \qquad \sum_{j\in\mathrm{VF}(i)} J_{ij}^R = 0, \quad i \neq i_a, i_b.$$

Finally, the transition rate from absorbing set A to B can be calculated from the current. It is shown in [MSVE09, Theorem 2.15] that the transition rate from A to B is given by

$$(4.18) \qquad k_{AB} = \sum_{i \in A} \sum_{j \in \mathrm{VF}(i)} J_{ij}^R.$$

Particularly, if there is only one point $\mathbf{y}_{i_a} \in A$, then

$$(4.19) \qquad k_{AB} = \langle Qq, \delta_{i_a} \rangle_\pi = \sum_{j \in \mathrm{VF}(i_a)} J_{i_a,j}^R,$$

where δ_{i_a} is the Kronecker delta with value 1 if $i = i_a$ while 0 otherwise.

4.2.2. Finite volume scheme and Q^q-matrix for controlled Markov chain. Similar to the controlled Markov process in (3.42), we give the controlled Markov chain on point clouds below. Suppose the local minima a and b of U are two cell centers with indices i_a and i_b. For simplicity, we assume there is only one point $\mathbf{y}_{i_a} \in \bar{A}$. We construct a controlled random walk on point clouds $\{\mathbf{y}_i\}_{i=1:n, i \neq i_a}$. The controlled random walk for the general case that more than one point belongs to A is similar. Below, we derive the master equation for this controlled random walk and still denote the density at states $\{\mathbf{y}_i\}_{i=1:n, i \neq i_a}$ as ρ_i.

The local minima a and b of U are our interest and usually the sampled data has high resolution near $a \in A$ and $b \in B$. Since our discrete Markov process Q^q is defined on the data cloud without points in A, we assume after taking out one of a few points in A, the remaining graph is assumed to be still connected. This assumption will be used in the spectral gap analysis for Q^q later.

First, with the effective potential U^e in (3.41), the effective equilibrium is $\pi^e = e^{-\frac{U^e}{\varepsilon}} = q^2 \pi$. We now construct a Markov process with a Q^q-matrix on states $\{\mathbf{y}_i\}_{i=1:n, i \neq i_a}$ such that

    (i) $\pi^e = q^2 \pi$ is an equilibrium;
    (ii) it satisfies the detailed balance $|C_i| \pi_i^e Q_{ij}^q = |C_j| \pi_j^e Q_{ji}^q$;
    (iii) it satisfies mass conservation $\frac{\mathrm{d}}{\mathrm{d}t} \sum_i \rho_i |C_i| = 0$.

Plug $\pi_i^e := q_i^2 \pi_i$ into the scheme (4.6). We propose a finite volume scheme for the controlled Fokker–Planck equation (3.42):

$$(4.20) \qquad \frac{\mathrm{d}}{\mathrm{d}t} \rho_i |C_i| = \sum_{j \in \mathrm{VF}(i), j \neq i_a} \frac{q_i q_j (\pi_i + \pi_j)}{2|y_i - y_j|} |\Gamma_{ij}| \left(\frac{\rho_j}{q_j^2 \pi_j} - \frac{\rho_i}{q_i^2 \pi_i} \right),$$
$$i = 1, \ldots, n, \ i \neq i_a.$$

With Q in (4.8), we define for $i = 1, \ldots, n, i \neq i_a$,

$$(4.21) \qquad Q_{ij}^q := \frac{q_j}{q_i} Q_{ij} \geq 0 \quad (i \neq j), \text{ and } Q_{ii}^q = - \sum_{j \neq i, i_a} Q_{ij}^q.$$

Q^q is an $n-1$ by $n-1$ Q-matrix which has zero row sum, i.e., $\sum_{j \neq i_a} Q_{ij}^q = 0, i \neq i_a$. One can recast (4.20) as a backward equation

$$(4.22) \qquad \begin{aligned} \frac{\mathrm{d}}{\mathrm{d}t} \frac{\rho_i}{\pi_i^e} &= \sum_{j \in \mathrm{VF}(i), j \neq i_a} \frac{q_j}{q_i} \frac{(\pi_i + \pi_j)}{2\pi_i |C_i| |y_i - y_j|} |\Gamma_{ij}| \left(\frac{\rho_j}{\pi_j^e} - \frac{\rho_i}{\pi_i^e} \right) \\ &= \sum_{j \in \mathrm{VF}(i), j \neq i_a} Q_{ij}^q \left(\frac{\rho_j}{\pi_j^e} - \frac{\rho_i}{\pi_i^e} \right), \quad i = 1, \ldots, n, \ i \neq i_a, \end{aligned}$$

and Q^q is the effective generator for the controlled Markov process on point clouds $\{\mathbf{y}_i\}_{i=1:n, i \neq i_a}$.

For (i), by plugging $\pi^e = q^2 \pi$ into (4.20), one obtains that π^e is an equilibrium solution.

For (ii), we can verify for $i, j \neq i_a$ and $i \neq j$

$$(4.23) \qquad |C_i| \pi_i^e Q_{ij}^q = q_i q_j \pi_i Q_{ij} |C_i| = q_i q_j \pi_j Q_{ji} |C_j| = |C_j| \pi_j^e Q_{ji}^q,$$

where we used the detailed balance property of Q.

For (iii), recast (4.20) as matrix form

$$(4.24) \qquad \begin{aligned} \frac{\mathrm{d}}{\mathrm{d}t} \rho_i |C_i| &= \sum_{j \in \mathrm{VF}(i), j \neq i_a} Q_{ij}^q \pi_i^e |C_i| \left(\frac{\rho_j}{\pi_j^e} - \frac{\rho_i}{\pi_i^e} \right) \\ &= \sum_{j \in \mathrm{VF}(i), j \neq i_a} \left(Q_{ji}^q |C_j| \rho_j - Q_{ij}^q |C_i| \rho_i \right). \end{aligned}$$

The summation with respect to i for both sides concludes mass conservation $\frac{\mathrm{d}}{\mathrm{d}t} \sum_{i \neq i_a} \rho_i |C_i| = 0$.

Second, we plug ρ_i^R defined in (4.15) into (4.20), and by using (4.14), we have

$$(4.25)$$
$$\sum_{j \in \mathrm{VF}(i), j \neq i_a} \frac{q_i q_j (\pi_i + \pi_j)}{2|y_i - y_j|} |\Gamma_{ij}| \left(\frac{1}{q_j} - \frac{1}{q_i} \right) = - \sum_{j \in \mathrm{VF}(i), j \neq i_a} \frac{\pi_i + \pi_j}{2|y_i - y_j|} |\Gamma_{ij}| (q_i - q_j) = 0,$$
$$i = 1, \ldots, n, \ i \neq i_a, i_b.$$

However, we emphasize that ρ^R is not an equilibrium for the proposed Markov process (4.20) because $Q_{i_b i_b}^q \neq Q_{i_b i_b}$.

Third, let us discuss the spectral gap of Q^q-matrix:

(1) From zero row sum property, we know 0 is an eigenvalue of Q^q.
(2) From the detailed balance property (4.23), we know the dissipation estimate

$$(4.26) \qquad \langle Q^q u, u \rangle_{\pi^e |C|} = -\frac{1}{2} \sum_{i,j; i \neq j} Q_{ij}^q (u_j - u_i)^2 \pi_i^e |C_i| \leq 0.$$

Thus the eigenvalues of Q^q satisfy $0 = \lambda_1 \geq \lambda_2 \geq \cdots$.

(3) Since the manifold $\mathcal{N}$ is assumed to be connected, the associated graph for Q given by Delaunay triangulation is connected. Based on the assumption that there are many sampled data nearby local minima a and b, we assume that after taking out i_a, the graph is still connected. Otherwise, with the help of the data-enrichment techniques mentioned in section 4.1.1, we can still assume that the Voronoi cell estimation is valid, and after taking out i_a, the graph associated with Q^q is still connected. Hence $\langle Q^q u, u \rangle_{\pi^e |C|} = 0$ if and only if $u \equiv$ constant. Therefore there is a spectral gap for Q^q, i.e., $0 = \lambda_1 > \lambda_2 \geq \cdots$.

Finally, one can recast (4.22) as the controlled Markov process with the controlled transition probability matrix (P_{ji}^q) (from site j to i) and the controlled jump rate $R^q = \mathrm{diag}(\lambda_j^q)$,

$$(4.27) \qquad \frac{\mathrm{d}}{\mathrm{d}t} \rho_i |C_i| = \sum_{j \in \mathrm{VF}(i), j \neq i_a} \lambda_j^q P_{ji}^q \rho_j |C_j| - \lambda_i^q \rho_i |C_i|, \quad i = 1, 2, \ldots, n, \ i \neq i_a,$$

where

$$\lambda_i^q := \sum_{j \neq i} Q_{ij}^q = \frac{1}{2|C_i|\pi_i} \sum_{j \in \mathrm{VF}(i), j \neq i_a} \frac{q_j}{q_i} \frac{\pi_i + \pi_j}{|y_i - y_j|} |\Gamma_{ij}|, \quad i = 1, 2, \ldots, n, \ i \neq i_a;$$

(4.28)
$$P_{ij}^q := \begin{cases} \dfrac{Q_{ij}^q}{\lambda_i^q} = \dfrac{1}{\lambda_i^q} \dfrac{q_j}{q_i} \dfrac{\pi_i + \pi_j}{2\pi_i |C_i|} \dfrac{|\Gamma_{ij}|}{|y_i - y_j|}, & j \in \mathrm{VF}(i), j \neq i_a; \\[2em] 0, & j \notin \mathrm{VF}(i). \end{cases}$$

We remark that the controlled generator Q^q (4.21) constructed using the Doob h-transform is also used in [Tod09, BH16] for the exit problem for controlled Markov chains; see also [GL20, GJL21] for the application in the image transformation and Bayesian inference. For more general chemical reaction processes represented as a time-changed jump process on countable states, we refer the reader to [GL22a, GL22c] for the optimal control formulation and the large deviation principle in the thermodynamic limit. However, designing the optimally controlled Markov chain for chemical reaction processes, particularly at finite noise level, is still open.

Under the constructed controlled transition probability matrix (P_{ij}^q) for the controlled random walk, the transition from the metastable state $a \in A$ to $b \in B$ is almost sure in $O(1)$ time rather than a rare event. Taking advantage of this nature, we will provide an algorithm for finding the mean transition path from A to B. This algorithm can be efficiently implemented by Monte Carlo simulation of the controlled random walk on point cloud. See Algorithm 2.

Remark 4.1. Similar to the continuous version, we formally calculate the discrete optimal control fields below. From (4.20),

(4.29) $\quad \dfrac{\mathrm{d}}{\mathrm{d}t} \rho_i |C_i| = (Q^q)^*(\rho|C|)$

$$:= \sum_{j \in \mathrm{VF}(i)} \frac{(\pi_i + \pi_j)}{2|y_i - y_j|} |\Gamma_{ij}| \left(\frac{q_i}{q_j} \frac{\rho_j}{\pi_j} - \frac{q_j}{q_i} \frac{\rho_i}{\pi_i} \right)$$

$$= \sum_{j \in \mathrm{VF}(i)} \frac{(\pi_i + \pi_j)}{2|y_i - y_j|} |\Gamma_{ij}| \left(\frac{\rho_j}{\pi_j} - \frac{\rho_i}{\pi_i} + \left(\frac{q_i}{q_j} - 1 \right) \frac{\rho_j}{\pi_j} - \left(\frac{q_j}{q_i} - 1 \right) \frac{\rho_i}{\pi_i} \right)$$

$$= \sum_{j \in \mathrm{VF}(i)} \frac{(\pi_i + \pi_j)}{2|y_i - y_j|} |\Gamma_{ij}| \left(\frac{\rho_j}{\pi_j} - \frac{\rho_i}{\pi_i} \right)$$

$$+ \sum_{j \in \mathrm{VF}(i)} \frac{(\pi_i + \pi_j)}{2|y_i - y_j|} |\Gamma_{ij}| \left(\frac{\rho_j}{q_j \pi_j} + \frac{\rho_i}{q_i \pi_i} \right) (q_i - q_j)$$

$$= Q^*(\rho|C|) - \sum_{j \in \mathrm{VF}(i)} |\Gamma_{ij}| \frac{q_j - q_i}{|y_i - y_j|} \frac{(\pi_i + \pi_j)}{2} \left(\frac{\rho_j}{q_j \pi_j} + \frac{\rho_i}{q_i \pi_i} \right)$$

$$= Q^*(\rho|C|) - \sum_{j \in \mathrm{VF}(i)} |\Gamma_{ij}| v_{ij} \rho_{ij},$$

where $v_{ij} = 2\frac{(q_j - q_i)}{|y_j - y_i|} \frac{2}{q_i + q_j}$ and $\rho_{ij} = \frac{1}{8}(q_i + q_j)(\pi_i + \pi_j)(\frac{\rho_j}{q_j \pi_j} + \frac{\rho_i}{q_i \pi_i})$. Thus, as a counterpart of Theorem 3.3, from the optimal control viewpoint for the Markov process (random walk) on point clouds, we can regard $v_{ij} = 2\frac{(q_j - q_i)}{|y_j - y_i|} \frac{2}{q_i + q_j}$ as the discrete optimal feedback control field from i to j (along edge e_{ij} of the associated Delaunay triangulation).

5. Data-driven solver and computations. In this section, we introduce the algorithms for finding the transition path on point clouds. As we will see, the transition from one metastable state to another for the optimally controlled Markov process is no longer rare. We can efficiently simulate these transition events and compute the mean transition path based on a level set determined by the committor function q and a mean path iteration algorithm on point clouds adapted from a finite temperature string method in [ERVE05]. Algorithms for the construction of the approximated Markov chain and the dominant transition path are given in section 5.1. Algorithms for the Monte Carlo simulation and the mean transition path based on the controlled Markov process are given in section 5.2.

5.1. Computation of dominant transition path. We first need to construct the approximated Markov chain based on the point clouds $\{\mathbf{y}_i\}_{i=1:n}$, i.e., to compute the coefficients in the discrete generator (4.8). In particular, the approximated cell volumes $|C_k|$ and the approximated edge areas $|\Gamma_{kl}|$ can be obtained by the approximated Voronoi tessellation in [GLW20, Algorithm 1]. Another related local meshed method for computing the committor function via point clouds was given in [LL18].

Then based on the associated Markov process (4.8) with the approximated coefficients, we can compute the dominant transition path and the transition rate between metastable states on manifold $\mathcal{N}$. Below we will simply mention the basic concepts and algorithms of the transition path theory of the Markov jump process for completeness. Further details can be found in [MSVE09].

We seek the dominant transition path from the starting state A to the ending state B. All algorithms presented are also valid for any starting state in absorbing set A and ending state in set B. This dominant path defined in [MSVE09] is the reactive path connecting A and B that carries the most probability current. We construct a weighted directed graph $G(V, E)$ using dataset $V = \{\mathbf{y}_i\}_{i=1:n}$ as nodes, $E = \{e_{ij}, J_{ij}^R > 0\}$ as a directed edge with weight J_{ij}^R. Here $J_{ij}^R > 0$ is computed via (4.16). From (4.16), there is no loop in the directed graph $G(V, E)$.

Given the starting and ending states $A, B \subset \{\mathbf{y}_i\}_{i=1:n}$, a reactive trajectory from A to B is an ordered sequence $P = [\mathbf{y}_0, \mathbf{y}_1, \ldots \mathbf{y}_k]$, $\mathbf{y}_i \in V$, $(\mathbf{y}_i, \mathbf{y}_{i+1}) \in E$ such that $\mathbf{y}_0 \in A$, $\mathbf{y}_k \in B$, and $\mathbf{y}_i \in (A \cup B)^c$, $0 < i < k$, for some $k \leq n$. We denote the set of all such reactive trajectories by $\mathscr{P}$. From (4.16), along any reactive trajectory $P \in \mathscr{P}$, the values of the committor function

$$(5.1) \qquad\qquad 0 = q_0 < q_1 < \cdots < q_k = 1$$

are strictly increasing from 0 to 1. Given a reactive trajectory P, the maximum current carried by this reactive trajectory P, called the capacity of P, is

$$c(P) := \min_{(i,j) \in P} J_{ij}^R.$$

Among all possible trajectories from A to B, one can further find the one with the largest capacity

$$(5.2) \qquad\qquad c_{\max} := \max_{P \in \mathscr{P}} c(P), \quad P_{\max} \in \operatorname{argmax}_{P \in \mathscr{P}} c(P).$$

We call the associated edge

$$(5.3) \qquad\qquad (b_1, b_2) = \operatorname{argmin}_{(i,j) \in P_{\max}} J_{ij}^R$$

the dynamical bottleneck with the weight $c_{\max} = J_{b_1 b_2}^R$. For simplicity, we assume J_{ij}^R are distinct, so b_1, b_2 are uniquely determined.

Finding the bottleneck provides a divide-and-conquer algorithm for finding the most probable path recursively. The dominant transition path is the reactive path with the largest effective probability current [MSVE09, EVE10]. Computing the dominant transition path is a recursion of finding the maximum capacity on subgraphs.

Now we use the bottleneck (b_1, b_2) and level-set of committor function q to divide the original graph $G(V, E)$ into two disconnected subgraphs G_L and G_R as below.

Note that every path in $P_{\max}$ passes through the bottleneck (b_1, b_2). Thus the weight of each edge in $P_{\max}$ is larger than the weight of bottleneck $J^R_{b_1 b_2}$. So we first remove all the edges of the original graph $G(V, E)$ with weight smaller than $J^R_{b_1 b_2}$. Denote

$$(5.4) \qquad V_L := \{\mathbf{y}_i; \ q_i \leq q_{b_1}\}, \quad V_R := \{\mathbf{y}_i; \ q_i \geq q_{b_2}\}.$$

Construct the new graph

$$(5.5) \qquad \begin{aligned} G_L &:= (V_L, E_L), \quad \text{with } E_L := \{e_{ij} \in E; \ \mathbf{y}_i, \mathbf{y}_j \in V_L, \ J^R_{ij} > J^R_{b_1 b_2}\}; \\ G_R &:= (V_R, E_R), \quad \text{with } E_R := \{e_{ij} \in E; \ \mathbf{y}_i, \mathbf{y}_j \in V_R, \ J^R_{ij} > J^R_{b_1 b_2}\}. \end{aligned}$$

Then we find the dominant transition path in G_L from A to b_1 and in G_R from b_2 to B. So the computation of the dominant transition path is simply finding the bottleneck recursively.

In summary, we will first compute the committor function q by solving the linear system (4.14). Then we construct the graph $G(V, E)$ and compute the dominant transition path based on recursively finding the bottlenecks and the dominant transition paths; see [MSVE09] for further implementation details of the algorithmic constructions.

5.2. Mean transition path and the computation on point clouds. The dominant transition path from metastable state A to B obtained by TPT is a transition path that carries the most probability current. Below we will introduce the concept mean transition path by taking expectation with respect to the transition path density (3.6), which forms the rationale of our algorithm.

For any codimension one surface S on $\mathcal{N} \subset \mathbb{R}^\ell$, we define its projected mean

$$(5.6) \qquad \boldsymbol{p}_S := \mathcal{P}\left(Z_S^{-1} \int_S x\pi(x)q(x)(1 - q(x)) \, \mathrm{d}\sigma\right),$$

where $Z_S = \int_S \pi(x)q(x)(1 - q(x)) \, \mathrm{d}\sigma$ is the normalization constant, and $\mathcal{P} : \mathbb{R}^\ell \to \mathcal{N}$ is a projection, e.g., the closest point projection, which is assumed to be unique in our paper. We denote the mean transition path by $\boldsymbol{p}(\alpha) \in \mathcal{N} \subset \mathbb{R}^\ell$, where $\alpha \in [0, 1]$ is the normalized arc length parameter that $|\boldsymbol{p}'(\alpha)| \equiv Const$.

First, notice from (5.1) that the committor function q strictly increases from 0 to 1 along the transition path $\boldsymbol{p}$ from A to B. We assume the manifold $\mathcal{N}$ can be parameterized by (q, σ). Second, choose S in (5.6) as the iso-committor surface intersecting $\boldsymbol{p}(\alpha)$:

$$(5.7) \qquad S_\alpha = \{x \in \mathcal{N} | q(x) = q(\boldsymbol{p}(\alpha))\}.$$

We define $\boldsymbol{p}(\alpha)$ as the projected mean on the iso-committor surface S_α. By the coarea formula on manifold, for any $\alpha \in [0, 1]$, we can rewrite (5.6) as

$$(5.8) \qquad \boldsymbol{p}(\alpha) = \mathcal{P}\left(Z_\alpha^{-1} \int_{\mathcal{N}} x\pi(x)|\nabla q(x)|\delta(q(x) - q(\boldsymbol{p}(\alpha))) \, \mathrm{d}x\right),$$

where we used that $q(x)$ is constant on S_α and is included in the normalization constant $Z_\alpha^{-1} := Z_{S_\alpha}^{-1} q(\boldsymbol{p}(\alpha))(1 - q(\boldsymbol{p}(\alpha)))$. We denote (5.8) as a projected average $\boldsymbol{p}(\alpha) = \mathcal{P} < x >_{\pi_{q(\boldsymbol{p}(\alpha))}}$, where the average is taken with respect to the density $\pi_{q(\boldsymbol{p}(\alpha))}(x) \propto \pi(x)|\nabla q(x)|\delta(q(x) - q(\boldsymbol{p}(\alpha)))$ on $\mathcal{N}$.

Note that in (5.8), the definition of $\boldsymbol{p}(\alpha)$ depends on $\boldsymbol{p}(\alpha)$ itself; we can compute $\boldsymbol{p}$ by a Picard iteration, i.e.,

$$(5.9) \quad \boldsymbol{p}^{l+1}(\alpha) = \mathcal{P}\left(Z_\alpha^{-1} \int x\pi(x)|\nabla q|\delta(q(x) - q(\boldsymbol{p}^l(\alpha)))\,\mathrm{d}x \right) := \mathcal{P}\langle x\rangle_{\pi_{q(\boldsymbol{p}^l(\alpha))}}.$$

This resembles the finite temperature string method [ERVE05, RVEME05], which is developed to compute the average of the right-hand side by sampling techniques. However, since the transition between metastable states rarely happens, the sampling is difficult.

With the help of the controlled dynamics dictated by effective potential U^e, one can compute the mean transition path $\boldsymbol{p}(\alpha)$ efficiently. Note that the optimally controlled equilibrium is only a modification of π with a prefactor, i.e., $\pi^e = Cq^2\pi$, where constant C ensures $\int_{\mathcal{N}} \pi^e\,\mathrm{d}x = 1$. Therefore, since $q(x)$ is constant on S_α, mean transition path $\boldsymbol{p}(\alpha)$ can be identically recast as

(5.10)
$$\boldsymbol{p}(\alpha) = \mathcal{P}\left((Z_\alpha C q^2(\boldsymbol{p}(\alpha)))^{-1} \int_{\mathcal{N}} x\pi^e(x)|\nabla q|\delta(q(x) - q(\boldsymbol{p}(\alpha)))\,\mathrm{d}x \right) =: \mathcal{P}\langle x\rangle_{\pi^e_{q(\boldsymbol{p}(\alpha))}}.$$

The density is $\pi^e_{q(\boldsymbol{p}(\alpha))} \propto \pi^e(x)|\nabla q|\delta(q(x) - q(\boldsymbol{p}(\alpha)))$. The mean transition path can be computed by Picard iteration:

$$(5.11) \qquad\qquad \boldsymbol{p}^{l+1}(\alpha) = \mathcal{P}\langle x\rangle_{\pi^e_{q(\boldsymbol{p}^l(\alpha))}}.$$

Under the dynamics governed by U^e, the exit from the attraction basin of metastable state A is almost sure in $O(1)$ time; thus the sampling of the transition is much easier.

On the numerical aspect, we can also compute $\boldsymbol{p}$ on point clouds. Given a point cloud $D = \{\mathbf{y}_i\}_{i=1:n}$, we simulate a random walk $\{\mathbf{y}_t^q\}$ on D based on the controlled generator Q^q in (4.21). In detail, we first extend the Markov process with $(Q^q)_{ij}$ in (4.21) to include the site i_a. Then we have $\lambda_{i_a}^q = +\infty$, so the waiting time at i_a is zero. Thus at $t = 0$, we start the simulation at $\mathbf{y}_0^q \in VF(i_a)$ with probability

$$(5.12) \quad P_{i_a j}^q = \frac{q_j(\pi_{i_a} + \pi_j)}{\mathcal{Z}} \frac{|\Gamma_{ji_a}|}{|y_{i_a} - y_j|}, \; j \in \mathrm{VF}(i_a), \quad \mathcal{Z} = \sum_{j \in \mathrm{VF}(i_a)} q_j \frac{\pi_{i_a} + \pi_j}{|y_{i_a} - y_j|} |\Gamma_{i_a j}|.$$

In other words, $P_{i_a j}^q \propto J_{i_a j}^R$. We refer the reader to [LN15, Lemma 1.3] for the reactive exit distribution on ∂A for the continuous Markov process. Suppose $\mathbf{y}_{t_k}^q = \mathbf{y}_i$; the next step is to update Δt_k and $\mathbf{y}_{t_{k+1}}^q$ as follows. (i) The waiting time $\Delta t_k = t_{k+1} - t_k \sim \mathcal{E}(\lambda_i^q)$ is an exponentially distributed random variable with rate λ_i^q; (ii) $\mathbf{y}_{t_k}^q$ jumps to $\mathbf{y}_j \in VF(\mathbf{y}_i)$ with probability $P_{ij}^q \equiv Q_{ij}^q/\lambda_i^q$, where λ_i^q is defined as in (4.11). We repeat this simulation K times to obtain the data $\{\mathbf{y}_k^q, \Delta t_k\}_{k=0:K}$, in which we restart the simulation from A each time when we hit B. Denote a sampled trajectory part P_r of length r, from ∂A to B, as $P_r := \{(\mathbf{y}_0^q, \Delta t_0), (\mathbf{y}_1^q, \Delta t_1), \ldots, (\mathbf{y}_r^q, \Delta t_r)\}$ such that $\mathbf{y}_0^q \in VF(i_a)$ and $\mathbf{y}_r^q \in B$. We summarize this simulation in Algorithm 1.

To implement the Picard iteration (5.11) using data set $\{\mathbf{y}_k^q, \Delta t_k\}_{k=0:K}$, we need to approximate the density $\pi^e_{q(\boldsymbol{p}(\alpha))}$ at first. We make an assumption that

---

Algorithm 1: Algorithm for controlled random walk on point clouds

---

Algorithm Inputs: Maximum iteration $K_{\max}$.

1. Set $k = 0$, $r = 0$. Generate $\mathbf{y}_0^q \in VF(i_a)$ with probability $P_{i_a j}^q$.
2. $\mathbf{y}_{k+1}^q := \mathbf{y}_{t_{k+1}}^q = \mathbf{y}_s$, where $s = \min\{s | \sum_{j=1, j \neq i}^s P_{ij}^q \geq \eta\}$, where $\eta \sim U[0,1]$ is a uniformly distributed random variable.
3. $t_{k+1} = t_k + \Delta t_k$, Δt_k being an exponentially distributed random variable with rate λ_i^q.
4. $k \leftarrow k+1$, $r \leftarrow r+1$. Repeat until $\mathbf{y}_r^q \in B$. Record the trajectory $P_r = \{(\mathbf{y}_0^q, \Delta t_0), \cdots, (\mathbf{y}_r^q, \Delta t_r)\}$.
5. Reset $r = 0$, $\mathbf{y}_r^q \in VF(i_a)$ according to Step 1. Repeat the above iterations until k exceeds the maximum iteration number $K_{\max}$.

$\pi_{q(\boldsymbol{p}(\alpha))}^e$ on S_α is localized in $\mathcal{B}_{r_0}^{\mathbb{R}^\ell}(\boldsymbol{p}(\alpha))$, the neighborhood of $\boldsymbol{p}(\alpha)$ with radius r_0 in Euclidean space $\mathbb{R}^\ell$, and $|\nabla q|$ is approximately constant in $\mathcal{B}_{r_0}^{\mathbb{R}^\ell}(\boldsymbol{p}(\alpha))$. Indeed, a similar assumption was also made in the construction of the finite temperature string method. With this assumption, $\langle x \rangle_{\pi_{q(\boldsymbol{p}(\alpha))}^e} \approx \langle x \rangle_{\tilde{\pi}_{q(\boldsymbol{p}(\alpha))}^e}$, where the density $\tilde{\pi}_{q(\boldsymbol{p}(\alpha))}^e(x) \propto \pi(x) \chi_{\mathcal{B}_{r_0}^{\mathbb{R}^\ell}(\boldsymbol{p}(\alpha))}(x)$. Taking advantage of ergodicity, we get

$$\langle x \rangle_{\pi_{q(\boldsymbol{p}(\alpha))}^e} \approx \frac{1}{T_\alpha} \sum_{k=0}^K \mathbf{y}_k^q \chi_{\mathcal{B}_{r_0}^{\mathbb{R}^\ell}(\boldsymbol{p}(\alpha))}(\mathbf{y}_k^q) \Delta t_k,$$

where $T_\alpha = \sum_{k=0}^K \Delta t_k \chi_{\mathcal{B}_{r_0}^{\mathbb{R}^\ell}(\boldsymbol{p}(\alpha))}(\mathbf{y}_k^q)$.

Numerically, we discretize $\boldsymbol{p}(\alpha), \alpha \in [0,1]$, into $P = \{p_m\}_{m=1:M}$ for some $M \in \mathbb{N}$. For the lth iteration step and for any p_m^l, we select segments of reactive trajectories inside the ball $\mathcal{B}_{r_0}^{\mathbb{R}^\ell}(p_m^l)$, where the radius $r_0 > 0$ is chosen such that $\{\mathbf{y}_k^q\} \cap \mathcal{B}_{r_0}^{\mathbb{R}^\ell}(p_m^l)$ has enough samples. Denote the resulting samples as

$$(5.13) \quad \{\mathbf{y}_k^q\}_{k=0:K} \cap \mathcal{B}_{r_0}^{\mathbb{R}^\ell}(p_m^l) = \{\mathbf{y}_{r_1}^q, \ldots \mathbf{y}_{r_s}^q\}, \quad r_1, r_2, \ldots, r_s \in \{0, 1, \ldots, K\},$$

and the Picard iteration before projection takes the form

$$(5.14) \qquad \tilde{p}_m^{l+1} := \frac{1}{\Delta T_l} \sum_{j=1}^s \mathbf{y}_{r_j}^q \Delta t_{r_j}, \qquad \Delta T_l = \sum_{j=1}^s \Delta t_{r_j}.$$

Furthermore, in order to avoid the issue that all M discrete points overlap and concentrate on a few points, an arc-length reparameterizing procedure similar to [ERVE02] is needed.

To do the reparameterization, we first compute

$$(5.15) \qquad S_1 = 0, \quad S_m = \sum_{j=2}^m |\tilde{p}_m^{l+1} - \tilde{p}_{m-1}^{l+1}|, \quad m = 2, \ldots, M.$$

Then the total length of $\tilde{P}^{l+1}$ is approximately S_M. We do the arc-length reparameterizations by linear interpolation as follows. (i) Denote $L_m := \frac{m-1}{M-1} S_M$, $m = 1, 2, \ldots, M$; (ii) find the index m' such that $S_{m'} \leq L_m < S_{m'+1}$; (iii) calculate the linear interpolation

$$(5.16) \qquad \hat{p}_m^{l+1} \approx \frac{L_m - S_{m'}}{S_{m'+1} - S_{m'}} \tilde{p}_{m'}^{l+1} + \frac{S_{m'+1} - L_m}{S_{m'+1} - S_{m'}} \tilde{p}_{m'+1}^{l+1}.$$

Algorithm 2: Finding mean transition path on point clouds generated by controlled random walk.

Algorithm Inputs: Simulation data $\{\mathbf{y}_k^q\}_{k=0:K}$, waiting time $\{\Delta t_k\}_{k=0:K}$, radius $r_0 > 0$.

1. Set $l = 0$ and for some M, initialize a discrete path $P^l = \{p_m^l\}_{m=1:M}$ on manifold $\mathcal{N}$ connecting A and B, where $p_m^l \in \mathcal{N}$.
2. For every $1 \leq m \leq M$, collect all sample points in $\mathcal{B}_{r_0}^{\mathbb{R}^\ell}(p_m^l)$ based on (5.13).
3. Update path $\tilde{P}^{l+1}$ with the projected average for $m = 1, \ldots, M$ via (5.14).
4. Compute $S_1, \ldots, S_M$ via (5.15).
5. Compute $\hat{p}_m^{l+1} = p_m^{l+1}$ by arc-length reparameterization (5.16).
6. Updating $P^{l+1} = \{p_m^{l+1}\}$ by finding the nearest point of each $\hat{p}_m^{l+1}$ in $\{\mathbf{y}_k^q\}_{k=0:K}$
7. $l \leftarrow l + 1$. Repeat until P^l converges or l exceeds a prescribed number $L_{\max}$.

Since we don't explicitly know the manifold, the projection step is done by updating p_m^{l+1} as the nearest point of $\hat{p}_m^{l+1}$ in data set $\{\mathbf{y}_k^q\}_{k=0:K}$. Then we can obtain the new path $P^{l+1} = \{p_m^{l+1}\}_{m=1:M}$. This updating process can be iteratively repeated until convergence, i.e., $P^{l+1} = P^l$ up to some tolerance. We summarize the above algorithm for finding the mean transition path in Algorithm 2.

Note that the Algorithm 2 only uses the local neighbors of each p_m^l in the data set $\{\mathbf{y}_k^q\}$. In contrast, the algorithm for finding dominant transition path, which is revisited in section 5.1, must consider the entire graph $G(V, E)$ with all of the nodes $\{\mathbf{y}_k\}$. So the proposed algorithm may be more efficient when the data set $\{\mathbf{y}_k^q\}$ is very large and most of the points are far away from the optimal transition path.

The Picard iteration method takes advantage of the controlled process that the transition from A to B happens easily. Our derivation of (5.11) shows that on the level set of $q(x)$, the sampling of the original dynamics can be replaced by the sampling of the controlled dynamics. Thus, compared with computing the average $\boldsymbol{p}(\alpha) = \mathcal{P}\langle x \rangle_{\pi_{q(\boldsymbol{p}(\alpha))}}$, the sampling cost is greatly reduced since the sample mean on the level set of $q(x)$ can be obtained easily (see (5.14)). Meanwhile, it also takes the benefit of the information of committor function $q(x)$. With the help of $q(x)$, the iteration is only applied to a fixed number of sample points and uses only the neighborhood of the discrete path. For instance, in the numerical examples in the next section, we only sample the controlled dynamics for 10^5 steps, which gives about 100 transitions. All the iterations are done based on these 10^5 sample points.

Similar to many other methods—for instance, the string method [ERVE02] and the finite temperature string method [ERVE05]—this Picard iteration method is a local method. When there are multiple reaction channels with similar probability, the method only converges to one of them. Which one the method will converge to depends on the initial path P^0. To deal with multiple reaction channels, one can generate multiple initial paths and apply the algorithm to get different convergent paths.

6. Numerical results. In this section, based on the mean transition path algorithms in section 5.2, we conduct three examples, including two examples of Muller potential and a real-world example for an alanine dipeptide with a full atomic molecular dynamics data.
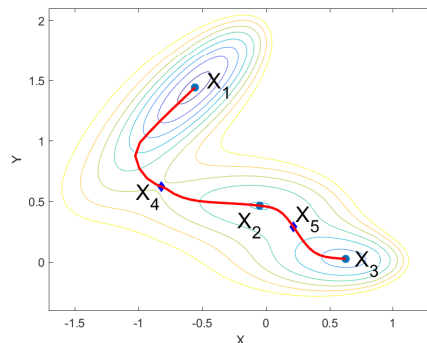
FIG. 1.   *Contour plot of* 2D *Mueller potential* $U(X, Y)$ *in* (6.1) *and transition path from* $\boldsymbol{X}_1$ *to* $\boldsymbol{X}_3$. *The blue dots are local minima* $\boldsymbol{X}_{1,2,3}$. *The blue diamonds are saddle points* $\boldsymbol{X}_{4,5}$. *The red line is the transition path obtained by string method.*

6.1. Synthetic examples of Mueller potential. We choose the Mueller potential on $\mathbb{R}^2$ as the illustrative example and map it to different manifolds. The Mueller potential on $\mathbb{R}^2$ is

$$(6.1) \quad U(X, Y) := \sum_{i=1}^{4} A_i \exp\left(a_i(X - \alpha_i)^2 + b_i(X - \alpha_i)(Y - \beta_i) + c_i(Y - \beta_i)^2\right).$$

The parameters are set to be $A_{1-4} = -2, -1, -1.7, 0.15$, $a_{1-4} = -1, -1, -6.5, 0.7$, $b_{1-4} = 0, 0, 11, 0.6$, $c_{1-4} = -10, -10, -6.5, 0.7$, $\alpha_{1-4} = 1, 0, -0.5, -1$, $\beta_{1-4} = 0, 0.5$, $1.5, 1$. Denote $\boldsymbol{X} = (X, Y)$. This potential has three local minima $\boldsymbol{X}_1, \boldsymbol{X}_2, \boldsymbol{X}_3$ and two saddle points $\boldsymbol{X}_4, \boldsymbol{X}_5$. The contour plot of the Mueller potential and the stationary points are shown in Figure 1.

We are interested in the transitions from the metastable state $\boldsymbol{X}_1$ to $\boldsymbol{X}_3$. Finding the transition path from $\boldsymbol{X}_1$ to $\boldsymbol{X}_3$ is a well-studied problem. One can compute the transition path by some existing methods like string method [ERVE02], etc., which is shown in Fig. 1.

Example 1: *Mueller potential on sphere.* We map the Mueller potential to $\mathcal{N} = \mathbb{S}^2$ by the stereographic projection $X = x/(1 - z)$, $Y = y/(1 - z)$. For any point $(x, y, z) \in \mathbb{S}^2$ except the north pole, we define $U_{\mathcal{N}}(x, y, z)$ on $\mathbb{S}^2$ as

$$U_{\mathcal{N}}(x, y, z) = U_{\mathbb{S}^2}(x, y, z) = U\left(\frac{x}{1 - z}, \frac{y}{1 - z}\right), \quad (x, y, z) \in \mathbb{S}^2,$$

and consider the transitions between two metastable states under the dynamics (1.1). It is easy to obtain that the invariant distribution of $\mathbf{y}_t$ is $\pi(\mathbf{y}) \propto \exp(-\varepsilon^{-1}U_{\mathbb{S}^2}(\mathbf{y}))$, $\mathbf{y} = (x, y, z)$. We then generate the data set $D = \{\mathbf{y}_i\}_{i=1:4000}$ uniformly on $\mathbb{S}^2$ and set $\pi_i = \exp(-\varepsilon^{-1}U_{\mathbb{S}^2}(\mathbf{y}_i))$, respectively. We choose the starting state $A = D \cap \mathcal{B}_{0.05}^{\mathbb{R}^3}(\boldsymbol{X}_1)$ and the ending state $B = D \cap \mathcal{B}_{0.05}^{\mathbb{R}^3}(\boldsymbol{X}_3)$, where $\mathcal{B}_r^{\mathbb{R}^3}(\boldsymbol{x}) = \{\mathbf{y} \in \mathbb{R}^3 | \|\mathbf{y} - \boldsymbol{x}\| < r\}$ is the ball centered at $\boldsymbol{x}$ with radius r in $\mathbb{R}^3$. With this data set, we can compute the committor function $q(\mathbf{y})$ by solving the approximated Voronoi tesselation and the linear system (4.14). Since it is a diagonally dominant system, the solution is unique, and we utilize a diagonal preconditioning trick to make the computation more effective and stable.

The effective potential U^e with $\varepsilon = 0.1$ is shown in Figure 2. Under the controlled random walk (4.27), the transition from A to B happens much more easily. One can
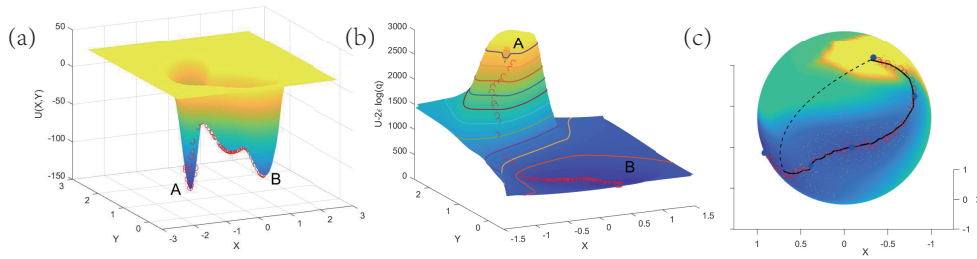
FIG. 2. *Projections of the Mueller potential and the effective potential on $\mathbb{S}^2$ to $\mathbb{R}^2$. (a) The projection of $U_{\mathbb{S}^2}(x,y,z)$ to $\mathbb{R}^2$. (b) The projection of effective potential $U^e = U_{\mathbb{S}^2} - 2\varepsilon \log q$ to $\mathbb{R}^2$. The contour lines of U^e are shown in colored lines. The hole at A is due to $U^e(A) = +\infty$. (c) The Monte Carlo simulation result of transition from A to B based on effective backward operator Q^q and the mean transition path. The background is a heat plot of U^e. The green dots are Monte Carlo samples. The black line is the mean transition path computed by Algorithm 2 while the dashed line is the initial discrete path. In all subfigures, the dominant transition paths are shown with red circles.*

see from the Monte Carlo simulation in Figure 2(c) that the exit from the attraction basin of metastable state $\boldsymbol{X}_1$ is almost sure rather than a rare event. Compared with the original $U_{\mathbb{S}^2}(\mathbf{y})$, in the effective potential, the local minimum at A disappears, and U^e tends to infinity when approaching A; see Figure 2(b). We can also find that the dominant transition path almost goes along the gradient direction of U^e from A to B. Taking the maximum iteration $K_{\max} = 10^5$ in the Monte Carlo simulation Algorithm 1, we find 48 transition trajectories from A to B; see Figure 2(c). In the simulation with the uncontrolled generator Q, there is no transition from A to B at all in 10^5 steps. The mean transition path based on Algorithm 2 is also shown using the solid black line in Figure 2(c). We set $M = 100$ and $L_{\max} = 20$ in the algorithm. The mean transition path derived by Monte Carlo simulation data (the solid black line in Figure 2(c)) highly coincides with the dominant transition path in TPT (red circles in Figure 2(c)). Providing rigorous justification for this remarkable coincidence is an important problem for future study. Indeed, both dominant transition path algorithm and mean transition path algorithm are designed to find "ensembles of transition paths" for fixed noise level $\varepsilon > 0$. Moreover, they both rely on the level-set of committor function q to order point clouds; see (5.4) and (5.7).

With committor function $q(\mathbf{y})$, we can obtain the dominant transition path by applying the TPT algorithms. We show the results for different ε in Figure 3(a)–(c). As a comparison, we also compute the minimum energy path in the limit $\varepsilon \to 0$. This can be done by minimizing the Freidlin–Wentzell action functional [FW12]. Namely, it is the solution of the following variational problem (i.e., (2.2)):

$$(6.2) \qquad S(B;A) = \inf_{T>0} \inf_{\boldsymbol{x} \in A, \boldsymbol{y} \in B} \inf_{\psi(t) \subset \mathcal{N}: \psi(0)=\boldsymbol{x}, \psi(T)=\boldsymbol{y}} \int_0^T \left\| \dot{\psi} + \nabla_{\mathcal{N}} U(\psi) \right\|^2 dt.$$

This problem can be efficiently solved by minimum action method (MAM) on the manifold [ERVE04, LLZ16]. Note that $U_{\mathbb{S}^2}(x,y,z)$ can be naturally extended to $\mathbb{R}^3 \backslash \{z = 1\}$, one can directly apply MAM on $\mathcal{N}$ by a properly designed MAM on $\mathbb{R}^3$. This zero-noise path is used as a reference; see solid red line in Figure 3. We also map the transition path on $\mathcal{N}$ to $\mathbb{R}^2$ by the stereographic projection. The result is shown in Figure 3(d)–(f).
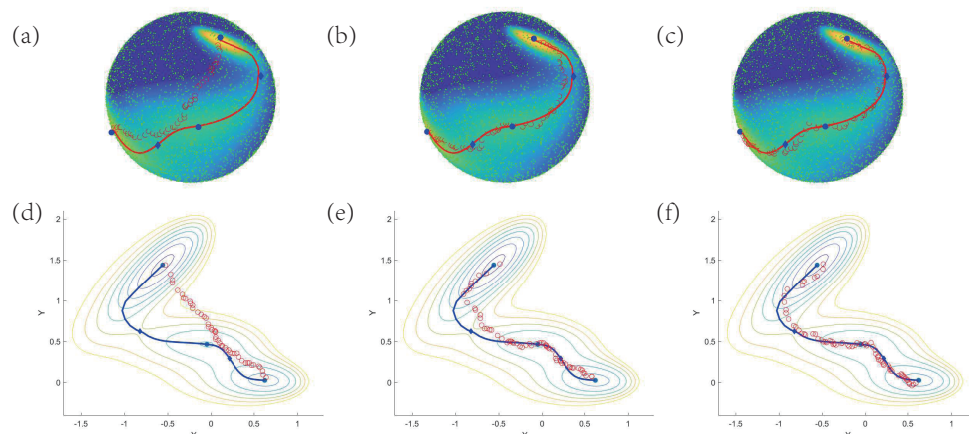
FIG. 3. *The dominant transition paths from $\boldsymbol{X}_1$ to $\boldsymbol{X}_3$ on $\mathbb{S}^2$ for different ε. (a), (d) $\varepsilon = 1$. (b), (e) $\varepsilon = 0.2$. (c), (f) $\varepsilon = 0.05$. In all subfigures, the blue dots are metastable states $\boldsymbol{X}_{1,2,3}$, while the blue diamonds are saddle points. (a)–(c) The background of each subfigure shows the heat plot of $U_{\mathbb{S}^2}(x, y, z)$. The small green dots are 4000 random samples. The paths of red circles are dominant transition paths obtained by TPT. The zero-noise minimum energy paths computed by MAM are shown with solid red lines. (d)–(f) The background is the contour plot of potential $U(X, Y)$. The solid blue lines and red circles are the projections of transition paths in (a)–(c), respectively.*

TABLE 1
Comparison of the transition rates obtained by TPT and the quasi-potential.

	$\varepsilon = 1$	$\varepsilon = 0.2$	$\varepsilon = 0.05$	$\varepsilon = 0.02$	$S(B; A)$
$-\varepsilon \log k_{AB}$	-0.4282	0.2540	0.3979	0.3999	0.3816

In Figure 3, we find that as ε tends to zero, the dominant transition path converges to the zero-noise path obtained by MAM both on manifold $\mathbb{S}^2$ and the 2D projection. This is consistent with the Freidlin–Wentzell theory. The results are stable when different random samples are utilized.

We can find some critical transition states along the dominant transition path with the help of probability current J^R. Note that finding the dominant transition path is a divide-and-conquer algorithm by finding a sequence of dynamical bottlenecks. The key transition states must have the least current J^R. In Figure 4, we plot the current J^R along the dominant transition path. The states with the least five J^R are marked and projected to $\mathbb{R}^2$, and ε is chosen to be 0.1. One can see that all of these five states are in neighborhoods of saddle points or local minima. As stated by the Freidlin–Wentzell theory, the transition path in the zero noise limit must pass through stationary points, which is confirmed in our computations.

The transition rate calculated by (4.18) is also consistent with the Freidlin–Wentzell theory. When A, B are metastable states, it is well known that as $\varepsilon \to 0$, $\varepsilon \log k_{AB} \to S(B; A)$, where $S(B; A)$ in (6.2) is the so-called quasi-potential. The value of $S(B; A)$ is a side product when computing the minimum energy path on manifold $\mathcal{N}$ by MAM. The rescaled logarithm of the rates k_{AB} for different ε and $S(B; A)$ are listed in Table 1. We can find that as ε becomes smaller, these two quantities get closer, as suggested by the theoretical result.
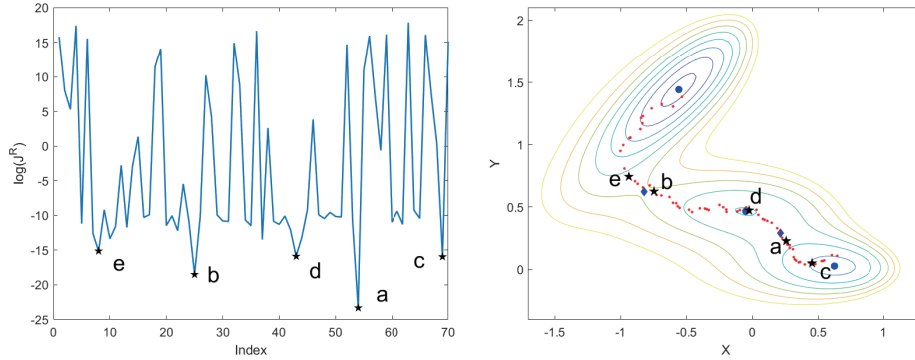
FIG. 4. *The key transition states along the dominant transition path, $\varepsilon = 0.1$. Left panel: The* $\log J^R$ *along the dominant transition path. The states with the least five J^R are marked by* a–e *in ascending order. Right panel: The projection of the dominant transition path on $\mathbb{R}^2$. This subfigure is similar to* (d)–(f) *of Figure* 3 *except that the dominant transition path is marked with red dots. The five states in the left panel are also marked in this subfigure.*

Example 2*: Mueller potential on torus.* We can also map the Mueller potential to the torus $\mathcal{N} = \mathbb{T}^2$, which is defined as

$$x = (R+r\cos\theta)\cos\phi, \quad y = (R+r\cos\theta)\sin\phi, \quad z = r\sin\theta, \quad \theta \in [-\pi, \pi), \phi \in [0, 2\pi).$$

Set $R = 2.0, r = 1.0$. We define the potential $U_{\mathcal{N}}$ on the torus as

$$U_{\mathcal{N}}(x, y, z) = U_{\mathbb{T}^2}(x, y, z) := U(r\theta, R\phi).$$

It is interesting to study the transition behavior of the dynamics (1.1) with finite but small noise, and the driving potential is also perturbed by noise with similar scales. In this case, minimizing the Freidlin–Wentzell action functional is not proper because the effect of finite noise is ignored. The finite temperature string method [ERVE05] is a good candidate for this problem. However, it is not straightforward to apply this method on a manifold.

Instead, we can still study this problem by TPT on point clouds. We perturb the Mueller potential by small oscillations as

$$\tilde{U}(X, Y) = U(X, Y) + 0.15\sin(10\pi X)\sin(10\pi Y)$$

and define the perturbed potential $U_{\mathcal{N}}$ on the torus by

$$U_{\mathcal{N}}(x, y, z) = \tilde{U}_{\mathbb{T}^2}(x, y, z) := \tilde{U}(r\theta, R\phi).$$

We choose $\varepsilon = 0.1$, which is in the same scale of our perturbations, and consider the transitions from $A = D \cap \mathcal{B}_{0.05}^{\mathbb{R}^3}(\boldsymbol{X}_1)$ to $B = D \cap \mathcal{B}_{0.05}^{\mathbb{R}^3}(\boldsymbol{X}_3)$. By using 4000 uniform random samples on $\mathbb{T}^2$, we obtain the dominant transition paths as shown with red circles in Figure 5. For a reference, we still plot the minimum energy path under zero noise and zero perturbation in (b).

We can find that the noise effect on the potential is eliminated, and we still capture the main transition behavior from $\boldsymbol{X}_1$ to $\boldsymbol{X}_3$. Although the landscape is rough, the density of transition path ρ^R is relatively smooth. The dominant transition path lies in the domain with the largest value of ρ^R.
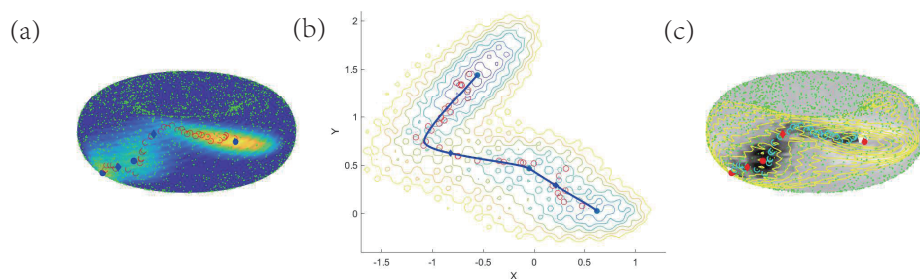
(a) (b) (c)

FIG. 5. *The dominant transition path from $\boldsymbol{X}_1$ to $\boldsymbol{X}_3$ on the torus under perturbed Mueller potential ($\varepsilon = 0.1$). In the three subfigures, the metastable states and saddle points are shown with blue dots and diamonds, respectively. (a) The background shows the heat plot of $\tilde{U}_{\mathbb{T}^2}(x, y, z)$. (c) The background shows the density of transition paths ρ^R in log scale. The yellow lines correspond to the contour of $\tilde{U}_{\mathbb{T}^2}(x, y, z)$. In subfigures (a) and (c), the small green dots are 4000 random samples, and the path of red/cyan circles is the dominant transition path. (b) The background is the contour plot of the perturbed Mueller potential $\tilde{U}(X, Y)$. The red circles and blue solid line correspond to the projection of the dominant transition path and the reference zero-noise minimum energy path, respectively.*
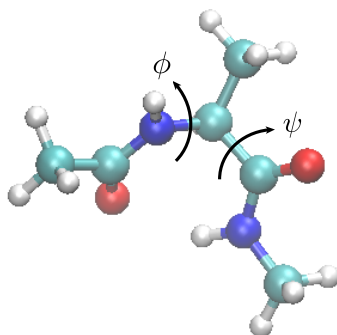

FIG. 6. *Schematic representation of the alanine dipeptide and two backbone dihedral angles ϕ and ψ.*

6.2. Application on an alanine dipeptide. We now apply our method to a computational chemistry problem, a manageable alanine dipeptide example with 22 atoms, with collected data from molecular dynamics (MD) simulation.

Example 3: *Application on alanine dipeptide in vacuum.* The alanine dipeptide in vacuum is a simple and well-studied molecule with 22 atoms, which implies $p = 66$. It has been shown that the lower energy states of alanine dipeptide can be mainly described by two backbone dihedral angles $\phi \in [-\pi, \pi)$ and $\psi \in [-\pi, \pi)$ (as shown in Figure 6); see [AFC99]. Thus, its configuration essentially lies on a torus $\mathcal{N}$, and the dynamics can be approximately governed by a stochastic equation like (1.1) with $\ell = 3$. The transition between different isomers of alanine dipeptide is a good example for the study of rare events.

We apply the full atomic MD simulation of the alanine dipeptide molecule in vacuum with the AMBER99SB-ILDN force field for 100ns with room temperature $T = 298K$. Then we collect the data (ϕ, ψ) directly from the MD result. The free energy $U_{\mathcal{N}}(\phi, \psi)$ is obtained from the MD simulation by the reinforced dynamics (Figure 7), which approximates $U_{\mathcal{N}}$ through a deep neural network and utilizes the
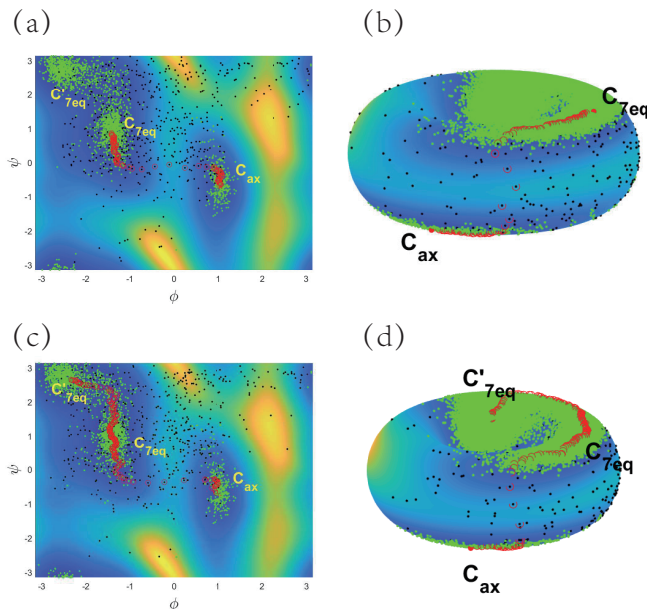
(a) (b)

(c) (d)

FIG. 7. *The sample points and transition paths from C_{ax} to C_{7eq} (subplot* (a)–(b)*) and C_{ax} to C'_{7eq} (subplot* (c)–(d)*). The green and black dots are MD and generated auxiliary sample points, respectively. The transition paths are marked by red circles. The background shows the effective potential $U_\mathcal{N}$ obtained by MD simulation.* (a), (c): *Visualization in the (ϕ, ψ) plane.* (b), (d): *Visualization on the torus.*

adaptive biasing force and reinforcement learning idea to encourage the space exploration [ZWE18]. There are three local minima, C_{ax}, C_{7eq}, and C'_{7eq}, corresponding to different isomers of alanine dipeptide. We will study the dominant transition paths from C_{ax} to C_{7eq}, and C_{ax} to C'_{7eq} in the following with the developed algorithms.

We collect $n = 50,000$ equidistant MD time series data $D = \{(\phi_{t_i}, \psi_{t_i})\}_{i=1:n}$ with $0 = t_0 < t_1 < \cdots < t_n$ $(t_{i+1} - t_i = \text{Const.})$ and map them to the torus $\mathcal{N} = \mathbb{T}^2 \subset \mathbb{R}^3$ by $\sigma : (\phi, \psi) \to (x, y, z)$ defined as

$$x_{t_i} = (R + r\cos\phi_{t_i})\cos\psi_{t_i}, \quad y_{t_i} = (R + r\cos\phi_{t_i})\sin\psi_{t_i}, \quad z_{t_i} = r\sin\phi_{t_i},$$

where $R = 2, r = 1$. These data are shown in Figure 7 (green dots). One can find that they concentrate around the metastable states and seldom appear in the transition region ($z \approx 0$ in Figure 7(b), (d)). To study the transition path, we need to do data enrichment by generating some auxiliary data.

We do this by interpolation in the following way. First, we find the indices $I = \{1 \le j \le n | z_{t_j} > 0, z_{t_{j+1}} < 0\}$ and collect two data sets $D^+ = \{(\phi_{t_i}, \psi_{t_i}) | i = j - 10, \ldots, j, j \in I\}$ and $D^- = \{(\phi_{t_i}, \psi_{t_i}) | i = j, \ldots, j + 10, j \in I\}$. Then we randomly select a pair of samples $(\phi_i^+, \psi_i^+) \in D^+$ and $(\phi_j^-, \psi_j^-) \in D^-$. An auxiliary sample $(\tilde{\phi}_i, \tilde{\psi}_i)$ is generated by $\tilde{\phi}_i = \beta_1\phi_i^+ + (1 - \beta_1)\phi_i^-$; $\tilde{\psi}_i = \beta_2\psi_i^+ + (1 - \beta_2)\psi_i^-$, where $\beta_{1,2} \sim \mathcal{U}[0, 1]$.

We sparsify the MD data points by randomly choosing 4,000 samples in D and generating 500 auxiliary samples $\{(\tilde{\phi}_i, \tilde{\psi}_i)\}_{i=1:500}$. Namely, the dataset we use to compute the dominant transition path is $\tilde{D} = \{\sigma(\phi_{t_i}, \psi_{t_i})\}_{i \in B} \cup \{\sigma(\tilde{\phi}_i, \tilde{\psi}_i)\}_{i=1:500} \subset \mathcal{N}$, where $B \subset \{1, 2, \ldots, n\}$ is a random batch with size 4000. The auxiliary samples
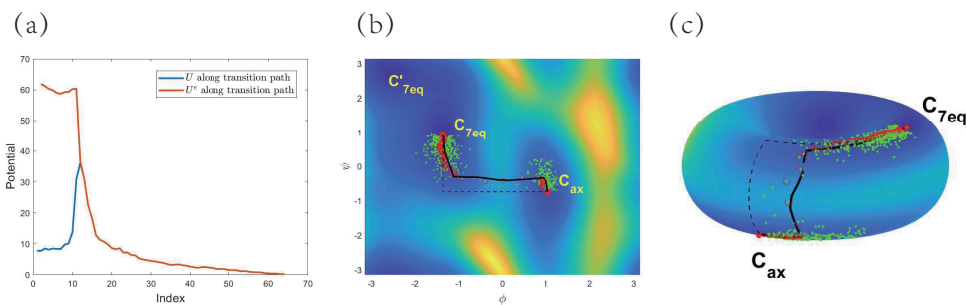
FIG. 8. *Numerical results for the transition from C_{ax} to C_{7eq} under the controlled process. (a) Comparison of $U_{\mathcal{N}}$ and effective potential U^e along the dominant transition path. (b)–(c) Simulation data of the controlled random walk (4.27) and the mean transition path obtained by Algorithm 2 with different visualizations (in the (ϕ, ψ) plane or on the torus). The green dots are Monte Carlo samples. The dominant transition path is shown in red circles. The black solid and dashed lines correspond to the mean transition path computed by Algorithm 2 and the initial path, respectively.*

are shown in Figure 7 with black dots. Applying TPT theory, we get the dominant transition path from C_{ax} to C_{7eq}, shown in Figure 7(a)–(b) with red circles. A similar approach can also be applied to obtain the dominant transition path from C_{ax} to C'_{7eq} (Figure 7(c)–(d)). Both results are consistent with previous studies on this problem using other methods [AFC99, RVEME05].

With the help of controlled random walk (4.27), we can simulate the transitions between the isomers more efficiently. We use the same dataset $\tilde{D}$ as in the previous computation and perform the simulation for studying the transition from C_{ax} to C_{7eq} by Monte Carlo Algorithm 1. The transition happens 21 times in $K = 10^5$ simulation steps. The potential $U_{\mathcal{N}}$ and effective potential U^e along the dominant transition path in Figure 7(a)–(b) are shown in Figure 8(a). Similarly to the case in Figure 2, the effective potential U^e achieves the local maximum at the C_{ax} state and approximately decreases to the C_{7eq} state. In contrast, the original potential $U_{\mathcal{N}}$ has a sharp local minimum at the C_{ax} state, which results in the rare transition from C_{ax} to C_{7eq}. This difference makes the transition under the potential U^e easy and frequent.

We then apply Algorithm 2 to get the mean transition path via the Monte Carlo samples of the controlled random walk. We set $M = 100$ and $L_{\max} = 200$ in Algorithm 2. The numerical results are shown in Figure 8(b)–(c). One can find that the mean transition path is perfectly consistent with the dominant transition path obtained by TPT.

7. Conclusion. In this paper, we first reinterpreted the transition state theory and the transition path theory as optimal control problems in an infinite time horizon. At a finite noise level $\varepsilon > 0$, based on the associated optimal control $v^* = 2\varepsilon \nabla \ln q$ and the controlled effective equilibrium $\pi^e = q^2 \pi$, we design an optimally controlled random walk on point clouds, which realizes the original rare events almost surely in $O(1)$ time scale. This enables an efficient sampling for the transitions between two conformational states in a biochemical reaction system. Taking advantage of the level set of the committor function q and the effective equilibrium $\pi^e = q^2 \pi$, a local averaging algorithm is proposed to compute the mean transition path on a manifold efficiently via the controlled Monte Carlo simulation data. Both synthetic and real-world examples are conducted to show the efficiency of the proposed algorithms, which gives results that are consistent with the dominant transition path algorithm. Rigorously

showing this consistency from the mathematical viewpoint is an interesting problem for future work.

REFERENCES

[AFC99]   J. Apostolakis, P. Ferrara, and A. Caflisch, *Calculation of conformational transitions and barriers in solvated systems: Application to the alanine dipeptide in water*, J. Chem. Phys., 110 (1999), pp. 2099–2108.

[BH16]   R. Banisch and C. Hartmann, *A sparse Markov chain approximation of LQ-type stochastic control problems*, Math. Control. Relat. Fields, 6 (2016), pp. 363–389.

[BKRS15]   V. Bogachev, N. Krylov, M. Röckner, and S. Shaposhnikov, *Fokker-Planck–Kolmogorov Equations*, Math. Surveys Monogr. 207, AMS , Providence, RI, 2015.

[CL06]   R. R. Coifman and S. Lafon, *Diffusion maps*, Appl. Comput. Harmon. Anal., 21 (2006), pp. 5–30.

[DS01]   J.-D. Deuschel and D. W. Stroock, *Large Deviations*, AMS, Providence, RI, 2001.

[ERVE02]   W. E, W. Ren, and E. Vanden-Eijnden, *String method for the study of rare events*, Phys. Rev. B, 66 (2002), 052301.

[ERVE04]   W. E, W. Ren, and E. Vanden-Eijnden, *Minimum action method for the study of rare events*, Comm. Pure Appl. Math., 57 (2004), pp. 637–656.

[ERVE05]   W. E, W. Ren, and E. Vanden-Eijnden, *Finite temperature string method for the study of rare events*, J. Phys. Chem. B, 109 (2005), pp. 6688–6693.

[EVE06]   W. E and E. Vanden-Eijnden, *Towards a theory of transition paths*, J. Stat. Phys., 123 (2006), pp. 503–523.

[EVE10]   W. E and E. Vanden-Eijnden, *Transition-path theory and path-finding algorithms for the study of rare events*, Ann. Rev. Phys. Chem., 61 (2010), pp. 391–420.

[Eva13]   L. C. Evans, *An Introduction to Stochastic Differential Equations*, AMS, Providence, RI, 2013.

[FS06]   W. H. Fleming and H. M. Soner, *Controlled Markov Processes and Viscosity Solutions*, 2nd ed., Springer, New York, 2006.

[FW12]   M. I. Freidlin and A. D. Wentzell, *Random Perturbations of Dynamical Systems*, Grundlehren Math. Wiss. 260, Springer, Berlin, Heidelberg, 2012.

[GL20]   Y. Gao and J.-G. Liu, *A note on parametric Bayesian inference via gradient flows*, Ann. Math. Sci. Appl., 5 (2020), pp. 261–282, https://doi.org/10.4310/AMSA.2020.v5.n2.a3.

[GL21]   Y. Gao and J.-G. Liu, *Random Walk Approximation for Irreversible Drift-Diffusion Process on Manifold: Ergodicity, Unconditional Stability and Convergence*, preprint, https://arxiv.org/abs/2106.01344, 2021.

[GL22a]   Y. Gao and J.-G. Liu, *Revisit of macroscopic dynamics for some non-equilibrium chemical reactions from a Hamiltonian viewpoint*, J. Stat. Phys., 189 (2022), 22, https://doi.org/10.1007/s10955-022-02985-5.

[GL22b]   Y. Gao and J.-G. Liu, *A Selection Principle for Weak Kam Solutions via Freidlin-Wentzell Large Deviation Principle of Invariant Measures*, preprint, https://arxiv.org/abs/2208.11860, 2022.

[GL22c]   Y. Gao and J.-G. Liu, *Thermodynamic Limit of Chemical Master Equation via Nonlinear Semigroup*, preprint, https://arxiv.org/abs/2205.09313, 2022.

[GJL21]   Y. Gao, G. Jin, and J.-G. Liu, *Inbetweening auto-animation via Fokker-Planck dynamics and thresholding*, Inverse Prob. Imaging, 15 (2021), pp. 843–864, http://doi.org/10.3934/ipi.2021016.

[GLW20]   Y. Gao, J.-G. Liu, and N. Wu, *Data-driven efficient solvers for Langevin dynamics on manifold in high dimensions*, Appl. Comput. Harmon. Anal., 62 (2023), pp. 261–309, https://doi.org/10.1016/j.acha.2022.09.003.

[GVE17]   T. Grafke and E. Vanden-Eijnden, *Non-equilibrium transitions in multiscale systems with a bifurcating slow manifold*, J. Stat. Mech.: Theory Exp., 2017 (2017), 093208.

[GVE19]   T. Grafke and E. Vanden-Eijnden, *Numerical computation of rare events via large deviation theory*, Chaos: Interdiscip. J. Nonlinear Sci., 29 (2019), 063118.

[HBS+13]   C. Hartmann, R. Banisch, M. Sarich, T. Badowski, and C. Schütte, *Characterization of rare events in molecular dynamics*, Entropy, 16 (2013), pp. 350–376.

[HRSZ17]   C. Hartmann, L. Richter, C. Schütte, and W. Zhang, *Variational characterization of free energy: Theory and algorithms*, Entropy, 19 (2017), 626.

[HS12]   C. HARTMANN AND C. SCHÜTTE, *Efficient rare event simulation by optimal nonequilibrium forcing*, J. Stat. Mech.: Theory Exp., 2012 (2012), P11004.

[HSZ16]   C. HARTMANN, C. SCHÜTTE, AND W. ZHANG, *Model reduction algorithms for optimal control and importance sampling of diffusions*, Nonlinearity, 29 (2016), pp. 2298–2326.

[HVE08]   M. HEYMANN AND E. VANDEN-EIJNDEN, *The geometric minimum action method: A least action principle on the space of curves*, Comm. Pure Appl. Math., 61 (2008), pp. 1052–1117.

[Kha12]   R. KHASMINSKII, *Stochastic Stability of Differential Equations*, Stoch. Model. Appl. Probab. 66, Springer, Berlin, Heidelberg, 2012.

[LL18]   R. LAI AND J. LU, *Point cloud discretization of Fokker–Planck operators for committor functions*, Multiscale Model. Simul., 16 (2018), pp. 710–726, https://doi.org/10.1137/17M1123018.

[LLZ16]   T. LI, X. LI, AND X. ZHOU, *Finding transition pathways on manifolds*, Multiscale Model. Simul., 14 (2016), pp. 173–206, https://doi.org/10.1137/140957780.

[LLL19]   A. LIU, J.-G. LIU, AND Y. LU, *On the rate of convergence of empirical measure in ∞-Wasserstein distance for unbounded density function*, Quart. Appl. Math., 77 (2019), pp. 811–829.

[LN15]   J. LU AND J. NOLEN, *Reactive trajectories and the transition path process*, Probab. Theory Relat. Fields, 161 (2015), pp. 195–244.

[MSVE06]   P. METZNER, C. SCHÜTTE, AND E. VANDEN-EIJNDEN, *Illustration of transition path theory on a collection of simple examples*, J. Chem. Phys., 125 (2006), 084110.

[MSVE09]   P. METZNER, C. SCHÜTTE, AND E. VANDEN-EIJNDEN, *Transition path theory for Markov jump processes*, Multiscale Model. Simul., 7 (2009), pp. 1192–1219, https://doi.org/10.1137/070699500.

[RVEME05] W. REN, E. VANDEN-EIJNDEN, P. MARAGAKIS, AND W. E, *Transition pathways in complex systems: Application of the finite-temperature string method to the alanine dipeptide*, J. Chem. Phys., 123 (2005), 052301.

[She85]   S.-J. SHEU, *Stochastic control and exit probabilities of jump processes*, SIAM J. Control Optim., 23 (1985), pp. 306–328, https://doi.org/10.1137/0323022.

[Tod09]   E. TODOROV, *Efficient computation of optimal actions*, Proc. Natl. Acad. Sci. USA, 106 (2009), pp. 11478–11483.

[TS15]   N. GARCIA TRILLOS AND D. SLEPČEV, *On the rate of convergence of empirical measures in ∞-transportation distance*, Canad. J. Math., 67 (2015), pp. 1358–1383.

[VEH08]   E. VANDEN-EIJNDEN AND M. HEYMANN, *The geometric minimum action method for computing minimum energy paths*, J. Chem. Phys., 128 (2008), 061103.

[Var07]   S. R. S. VARADHAN, *Stochastic Processes*, AMS, Providence, RI, 2007.

[Ver97]   A. YU. VERETENNIKOV, *On polynomial mixing bounds for stochastic differential equations*, Stochastic Process. Appl., 70 (1997), pp. 115–127.

[ZWE18]   L. ZHANG, H. WANG, AND W. E, *Reinforced dynamics for enhanced sampling in large atomic and molecular systems*, J. Chem. Phys., 148 (2018), 124113.